Journal of African Earth Sciences 213 (2024) 105205

Contents lists available at ScienceDirect

Journal of African Earth Sciences

journal homepage: www.elsevier.com/locate/jafrearsci

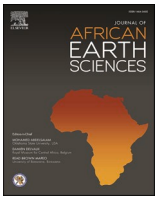

Integrated multi-proxy source-to-sink analysis of Late Barremian (Lower Cretaceous) clastic systems in the Essaouira-Agadir Basin

Emmanuel Roquette [a], James Lovell-Kennedy [a,#], Leonardo Muniz Pichel [a,1], Stefan Schröder [a,b], Rémi Charton [a,c,*], Ian Millar [d], Camille Frau [a,e], Jonathan Redfern [a,b]

[a] North Africa Research Group, The University of Manchester, England, UK
[b] Basin Studies, School of Earth and Environmental Sciences, The University of Manchester, England, UK
[c] Department of Geoscience and Engineering, Delft University of Technology, the Netherlands
[d] British Geological Survey, Keyworth, Nottinghamshire, England, UK
[e] Groupement d'Intérêt Paléontologique, Science et Exposition, 60 bd Georges Richard, 83000, Toulon, France

ARTICLE INFO

Handling Editor: Dr Mohamed Mohamed G Abdelsalam

Keywords:
Source-to-sink
Provenance analysis
Bouzergoun formation
Lower cretaceous
Barremian
Morocco
Essaouira agadir basin
Detrital zircon geochronology
Low-temperature thermochronology
Provenance
Paleogeology modelling
Hinterland evolution

ABSTRACT

This study investigates the provenance of the continental and marine Late Barremian clastics of the Bouzergoun Formation, exposed in the Essaouira-Agadir Basin (EAB). Thin section petrography, Scanning Electron Micrography, heavy minerals analysis, and detrital zircon dating were conducted and integrated with a large dataset of published Low-Temperature Thermochronology (LTT) studies to reconstruct the associated source-to-sink system (s). The results constrain the source and size of the system, and composition of deposited clastics, and investigate the mechanism for delivery of coarse clastics into the offshore domain, a key target for hydrocarbon exploration.

The homogeneity of rock composition fingerprints throughout the basin indicates a common provenance for both the northern and southern studied transects. Hinterland analysis based on LTT data identifies the Western Meseta and Massif Ancien de Marrakech (MAM) regions as the only possible source candidates exhuming during the Late Barremian, confirmed by detrital zircon geochronology. Heavy mineral populations reveal partly recycled sediment including a probable igneous source. Rock fragment populations comprise limestones, sandstones, and volcanic composition, which correlate with lithologies of the MAM.

The integration of all data suggests a best-fit model for the Late Barremian of a source-to-sink system of moderate size (200–300 km long), dominantly sourced from the MAM (western High Atlas). This provided a sand-rich mix of sediment resulting from the erosion of exhuming Triassic continental basins, with associated clays from the weathering of basalts and Triassic/Jurassic mudstones.

Late Barremian eustatic sea level fall, together with regional uplift in the hinterland, is interpreted to have resulted in a forced regression that allowed the system to prograde towards the slope margin, offering enhanced potential for sand delivery into the deep offshore domain. Seismic imaging offshore provides tentative interpretation of synchronous high reflectivity deepwater channels located in structural lows controlled by diapiric salt movement.

The Mesetian domain was likely undergoing denudation at the same time and shedding clastic-rich sediments to the northern part of the EAB, beyond the studied region. Sediment supply from the MAM may be mixed with the Mesetian sands to the northern part of the EAB and tentatively in the offshore Essaouira.

* Corresponding author. North Africa Research Group, the University of Manchester, England, UK.
E-mail addresses: emmanuel.roquette@gmail.com (E. Roquette), j.m.lovell-kennedy@liverpool.ac.uk (J. Lovell-Kennedy), leonardo.m.pichel@uib.no (L. Muniz Pichel), stefan.schroeder@manchester.ac.uk (S. Schröder), r.j.g.charton@tudelft.nl (R. Charton), ilm@bgs.ac.uk (I. Millar), camille_frau@hotmail.fr (C. Frau), jonathan.redfern@manchester.ac.uk (J. Redfern).
Current address: Department of Earth, Ocean and Ecological Sciences, University of Liverpool, England.
1 Current address: Department of Earth Science, University of Bergen, Bergen, Norway.

https://doi.org/10.1016/j.jafrearsci.2024.105205
Received 31 July 2023; Received in revised form 13 February 2024; Accepted 13 February 2024
Available online 4 March 2024

1. Introduction

This study uses a combination of published low-temperature thermochronology and new petrography, SEM, heavy mineral analysis, and detrital zircon geochronology data to constrain the geodynamics of the Essaouira-Agadir Basin (EAB) and its hinterland during the Late Barremian. The aim is to correlate probable sources of sediment in the hinterland, and to evaluate the origin and composition of sands being shed to the onshore and ultimately the offshore basin, with implications for reservoir prospectivity.

The Cenozoic Atlasic orogeny eroded large areas of the hinterland and transformed the paleo-topography and drainage systems. Within the mudstone-dominated Lower Cretaceous succession of interest, exposed in the onshore EAB, recent studies have identified a forced regression associated with an important clastic interval (Luber, 2017, Jaillard et al., 2019a, 2019b; Giraud et al., 2020; Bryers et al., this issue; see also discussion in Luber et al., this issue), dated to the Late Barremian interval.

Seismic imaging of the Jurassic and Cretaceous deep-water intervals offshore Morocco is complicated by salt deformation. The temporal and spatial distribution of sandstones within the deep basin, the main target for reservoirs for hydrocarbons, remain uncertain, and assessment of fluvial feeder input locations and sediment type are critical for future de-risking of exploration targets.

2. Geological setting

2.1. The essaouira-agadir basin

The Essaouira-Agadir Basin (EAB) is located in western Morocco (Fig. 1), at the junction of the western High Atlas rift basin and the Atlantic Margin. The EAB is bordered to the north by the western Meseta, to the south by the Souss Basin and Anti-Atlas and to the east by the Massif-Ancien de Marrakech (westernmost High Atlas; Behrens et al., 1978; Luber et al., 2017).

Rifting of the Central Atlantic occurred from the Middle Triassic to Early Jurassic. Triassic syn-rift continental red beds and evaporites (Beauchamp, 1988) are followed by passive margin shallow marine carbonates of Jurassic age (Adams, 1979; Frizon de Lamotte et al., 2008, Duval et al., this issue). Gradual deepening occurred between the Tithonian and early Albian (Butt, 1982; Nouidar and Chellai, 2000; Rey et al., 1986a, Duval et al., this issue), with the transition from shallow to deep shelf deposits (Fig. 2).

During the Lower Cretaceous, the EAB was a low-relief embayment, commonly referred to as the "Atlasic Gulf" (Behrens et al., 1978; Rey et al., 1986a, 1988). The EAB formed a shallow dipping shelf, open to the ocean in the west (Rey et al., 1988), which inherited its paleo-topography from the underlying Upper Jurassic to Lowermost Cretaceous (Berriasian) carbonate ramp (Luber, 2017).

The onshore Lower Cretaceous section is dominated by mudstones and subordinate, but significant, intervals of sandstone (Luber, 2017). A significant reduction in carbonate production is observed compared to the Jurassic (Wiedmann et al., 1978). Within the Atlasic Gulf the Lower Cretaceous stratigraphy thickens towards the opening Central Atlantic ocean to the west and thins towards the continent to the east (e.g., Rey et al., 1988; Zühlke et al., 2004; Ferry et al., 2007), a trend that is also observed at the stage level (e.g., Jaillard et al., 2019a, b; Reboulet et al., 2022). Significant thinning is recognized over some salt diapir structures (e.g., Tidzi diapir) and pre-existing paleo-topographic features (e.g., Cap Ghir, Amsittene, and Immouzer evaporite-cored anticlines previously reported by Rey et al., 1986b, 1988; Charton et al., 2021b, see reference therein).

Offshore, the EAB is characterised by syn-rift Triassic fluvio-continental sediments and Late Triassic/Jurassic evaporites covered by a c. 6–7.5 km (c. 5–6 s TWT) Meso-Cenozoic thick overburden (Pichel et al., 2019). Salt movement was coeval with Mesozoic sedimentation leading to intense deformation of the stratigraphic secession, with formation of 4–5 km tall diapirs and mini basins, as well as toe-fold-thrust

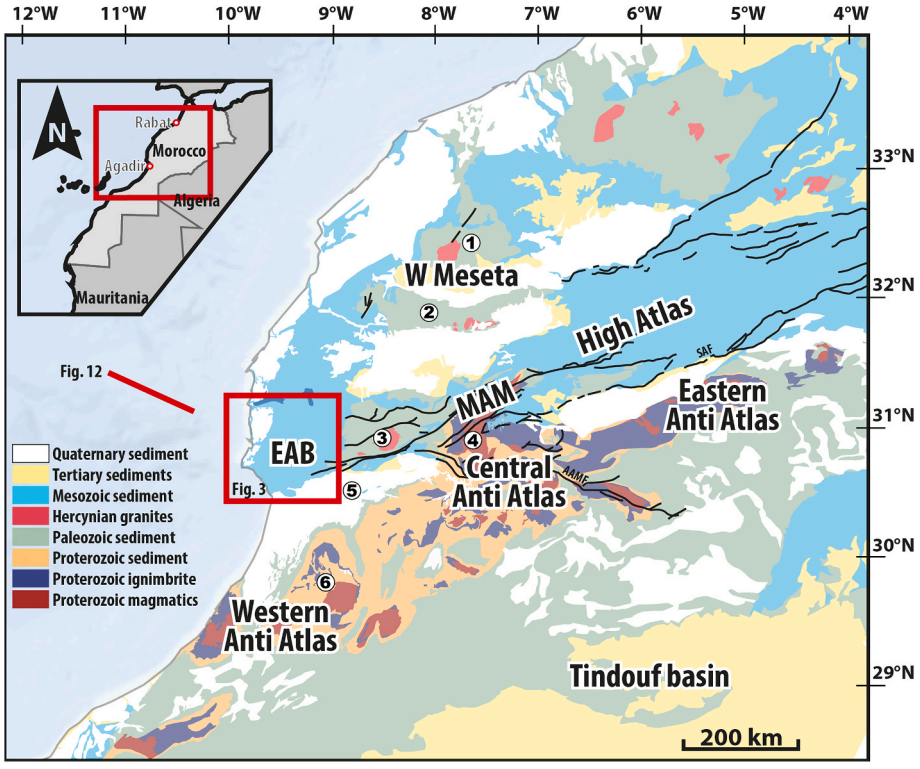

Fig. 1. Location of the study (red box) and simplified geological map of the hinterland of the Essaouira-Agadir Basin (EAB) (modified from Saadi et al., 1985). 1: Rehamna, 2: Jebilets, 3: Tichka Massif, 4: Siroua, 5: Souss Basin, 6: Kerdous massif, SAF: South Atlas Front, AAMF: Anti-Atlas Major Front.

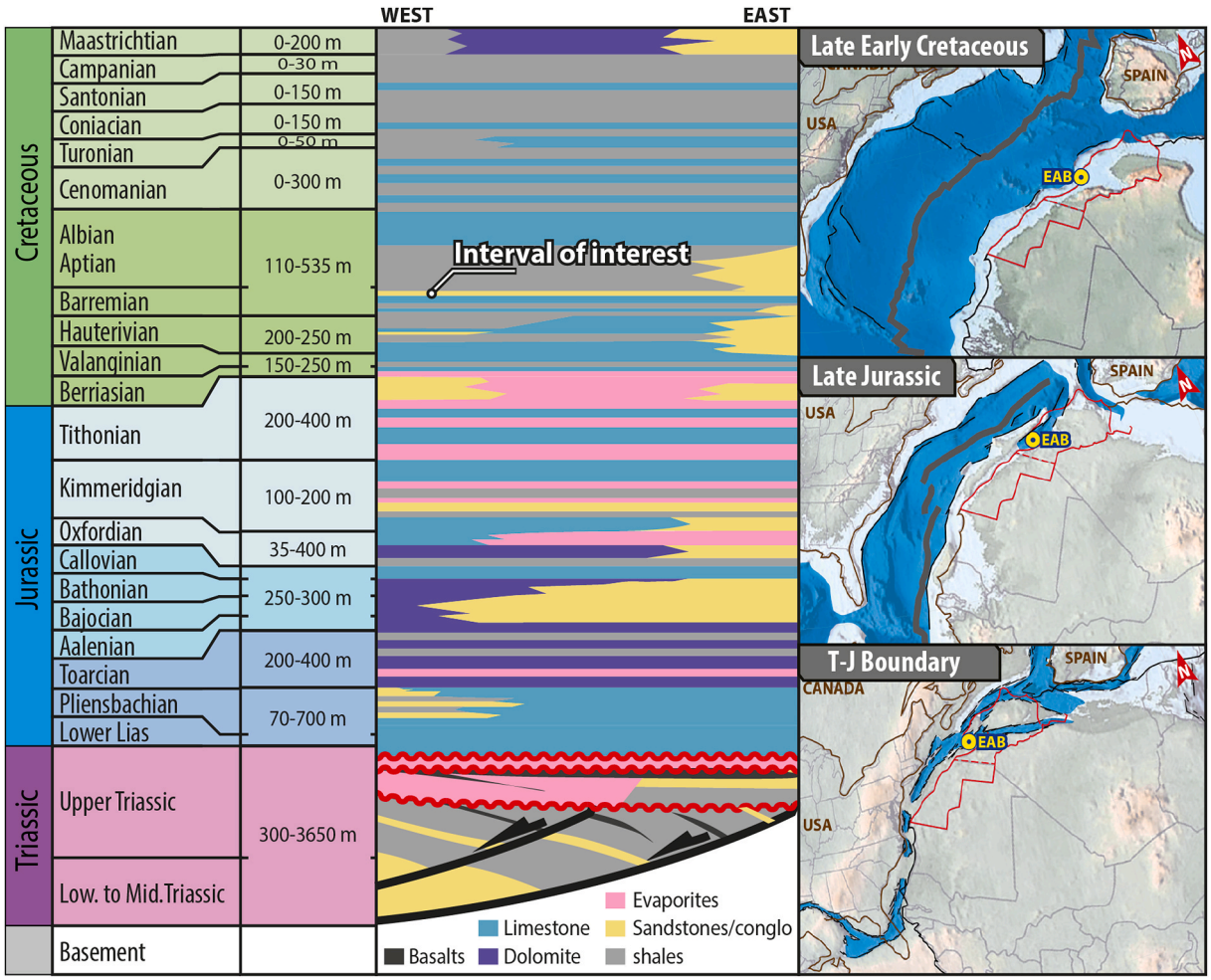

Fig. 2. Regional stratigraphic chart of the onshore Essaouira-Agadir Basin, modified from Frizon de Lamotte et al. (2008) and Triassic/Cretaceous tectonic evolution of the Central Atlantic, modified from reconstructions of PALEOMAP project (Scotese, 2016).

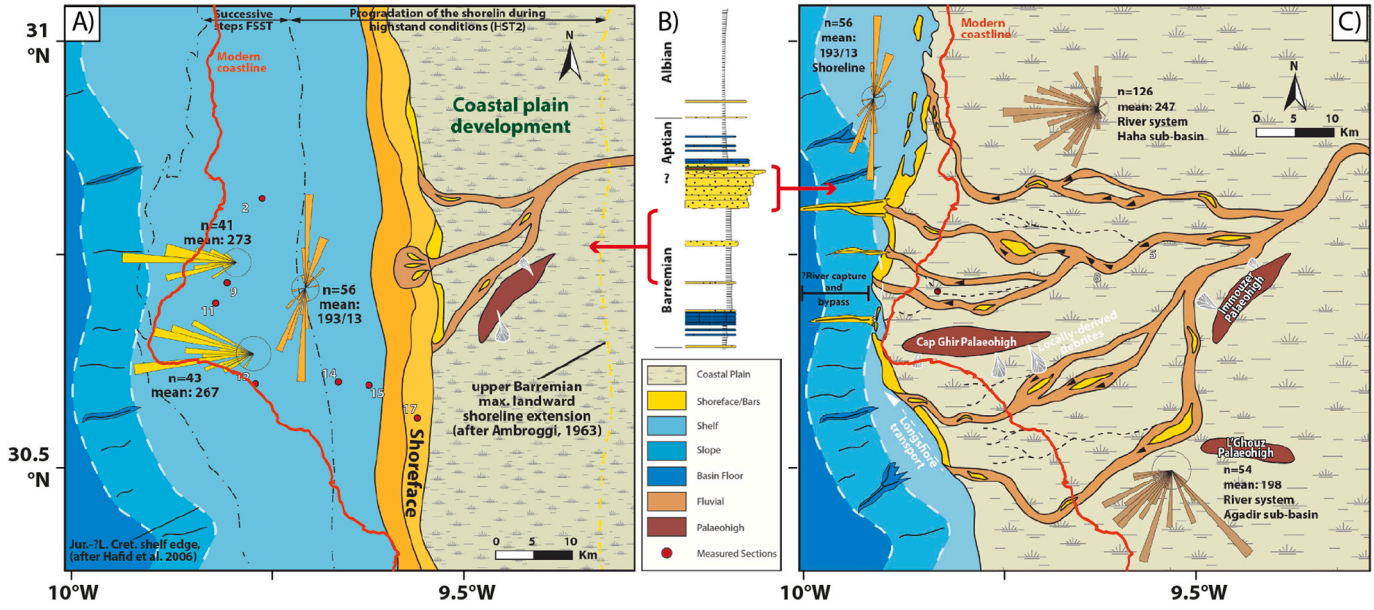

Fig. 3. A) Barremian HST2 highstand and C) Late Barremian regression, red-line = modern shoreline, modified from Luber (2017), shelf edge from (Hafid et al., 2006). B) Schematic profile of part of the Lower Cretaceous stratigraphy in the central EAB (Luber, 2017 and reference therein; yellow: sandstone, blue: limestone, white: marls). Note that the reconstructions show only Present-day longitudes and latitudes.

systems and canopy complexes (Tari et al., 2014; Pichel et al., 2019).

Recent studies have documented major exhumation events in western Morocco during the Middle Jurassic to Early Cretaceous (Barbero et al., 2007, 2011; Bertotti and Gouiza, 2012; Charton et al., 2021a; Ghorbal et al., 2008; Saddiqi et al., 2009; Domènech et al., 2018). Areas between the Precambrian Reguibat Shield (located south of the Tindouf Basin) and the Meseta in the north (Fig. 1) were affected by km-scale burial/exhumation events, which contrasts with models for post-rift thermal evolution expected along passive margins (Bertotti and Gouiza, 2012). The western High Atlas domain was also later uplifted and exhumed during the Cenozoic, with an acceleration from about 10 Ma ago (e.g., Lanari et al., 2020), that resulted in erosion and exposure of the Cretaceous sediments in the EAB.

2.2. Late Barremian

Within the mudstone-dominated Lower Cretaceous succession (see Ferry et al., 2007 for a synthesis of lower Cretaceous deposits of the EAB), an important phase of clastic input occurred in the Late Barremian (e.g., Nouidar, 2001, 2002; Luber, 2017; Luber et al., 2019; Jaillard et al., 2019a, b; Giraud et al., 2020) (Fig. 3). The Barremian is characterised by a long-term falling sea level trend (Haq, 2013). This interval is part of the Bouzergoun Formation and is well exposed onshore in the EAB. It is composed of shelf limestones and marine marls at the base, becoming increasingly clastic dominated towards the top, with fine grained shallow marine sandstones, coarse grained shallow marine sandstones (marginal-littoral), vari-coloured siltstone and mudstones, and marine to fluvial sandstones and conglomerates, (Rey et al., 1986a; Luber, 2017; Jaillard et al., 2019a and references therein; Luber et al., this issue). This prominent siliciclastic interval is interpreted as recording a forced regression, due to tectonic uplift of the hinterlands, as proposed by Luber (2017) and Jaillard et al. (2019a). Massifs in the EAB hinterlands (Meseta, MAM, and Anti-Atlas) were all undergoing exhumation at this time, around 125 Ma, which supplied the basin with important volume of sediments. Over this period a period marked by a shift of sedimentary sources is observed from the Meseta/MAM (Barremian) to the Anti-Atlas (Charton et al., 2021a; Luber et al., this issue), Subsidence curves from well data show the onset of uplift in the EAB at ~127 Ma (Le Roy and Piqué, 2001). Together with the global eustatic sea level fall, this is interpreted to be the driver for shoreline shift toward the shelf-edge, potentially enhancing the delivery of coarse siliciclastics directly to the deepwater basin (Luber, 201; Jaillard et al. (2019a); Fig. 3). This makes the Late Barremian interval the most favourable candidate for deep-water sandstone reservoirs in the offshore basin during the Lower Cretaceous.

The upper part of the Bouzergoun Formation transitions from shelfal muds with minor sandstones to shallow-marine, deltaic and fluvial sand-rich deposits (Luber, 2017; Jaillard et al., 2019a), with identified erosional channels and valley features. Paleocurrent measurements presented on Figs. 3B and 4 were acquired by Luber (2017) from fluvial cross beds, sole marks at the base of mouthbar deposits and symmetric wave-ripples. The data suggests an overall western to southwestern orientation of the fluvial system and, although limited to the available outcrops, a north-south orientation of the shoreline and associated offshore currents during the Barremian-Aptian (Nouidar and Chellai, 2000; 2002; Luber, 2017).

2.3. Zircon record from crystalline basement

In northwest Africa, crystalline basement outcrops in parts of the West African Craton (WAC). The WAC is divided into 3 domains separated by 2 intra-cratonic basins, from north to south, (1) the Anti-Atlas belt, (2) the Tindouf Basin, (3) the Reguibat Shield, (4) the Taoudeni Basin and (5) the Man-Leo Shield. The oldest rocks of the WAC are Archean in age, found within the Man-Leo and Reguibat Shields, which record crustal growth from 3.5 to 3.0 Ga as part of the Leonian and Liberian orogenic cycles (Potrel et al., 2007). The next major period of zircon formation was during the Paleoproterozoic Eburnean-Birimian orogeny, which impacted the Reguibat Shield and formed the basement of the Anti-Atlas mobile belt (Boher et al., 1992; Gasquet et al., 2008a) and the Moroccan Meseta (El Houicha et al., 2018).

A subsequent significant period of tectonic quiescence occurred, with no known zircon formation within the basement of the WAC and more broadly across north-west Africa. The “Mesoproterozoic gap” is a diagnostic feature of the zircon record of Gondwana (Ghienne et al., 2018; Stephan et al., 2019). During the Neoproterozoic, on the northern margin of the WAC, the Anti-Atlas was involved in the Pan-African orogeny. The Pan-African orogeny led to the addition of numerous granitoids into the crust of NW Africa (Gasquet et al., 2008a; Soulaimani et al., 2018). The final period of crustal growth along the North African margin was the Variscan Orogeny (Hoepffner et al., 2005). During the Variscan Orogeny, Carboniferous-Permian aged granites were intruded into the Moroccan Meseta and MAM; no granites of Variscan age are known south of the South Atlas Fault (Hoepffner et al., 2006; Michard et al., 2008a,b; Mrini et al., 1992).

In summary, the basement of the WAC has 3 possible age signals that can be identified from zircon dating.

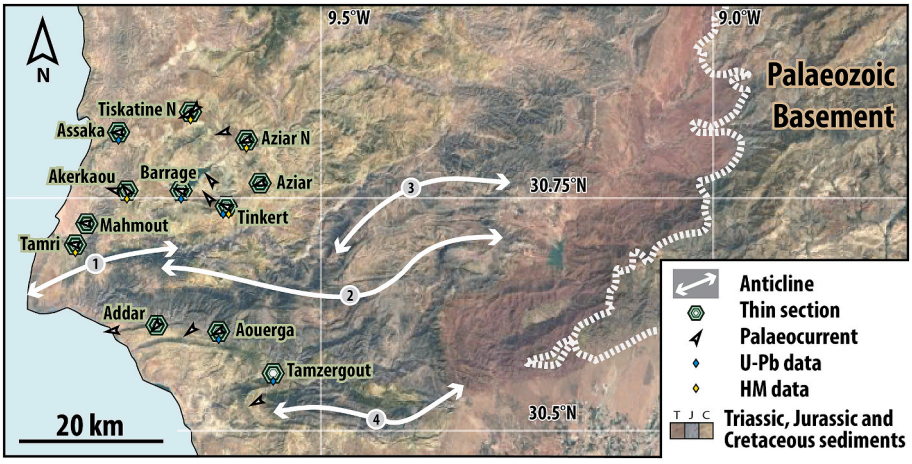

Fig. 4. Overview of the Essaouira-Agadir Basin. Background: satellite picture and topography data (Google Earth © Data SIO, NOAA, U.S. Navy, NGA, GEBCO Landsat/Copernicus Data), paleocurrents from Luber (2017); 1: Cap Ghir anticline, 2: Anklout anticline, 3: Imouzzer anticline, 4: Lgouz anticline.

1. Southern WAC signal: Archean and Paleoproterozoic grains corresponding to the Leonian-Liberian Orogeny (3.5–3.0 Ga) and the Eburnean-Birimian Orogeny (2.3–1.7 Ga).
2. Northern WAC and Anti-Atlas signal: Paleoproterozoic and Neoproterozoic populations corresponding to the Eburnean-Birimian orogeny (2.3–1.7 Ga) and the Pan-African Orogeny (0.8–0.54 Ga)
3. Moroccan Meseta signal: Neoproterozoic and Palaeozoic zircon populations corresponding to the Pan-African Orogeny (0.8–0.54 Ga) and the Variscan Orogeny (0.36–0.25 Ga).

2.4. Detrital zircon record

Due to the high stability of zircon grains through multiple sedimentary cycles (Andersen, 2005; Andersen et al., 2016; Morton, 1984), older sedimentary rocks are important potential sources of recycled zircon, especially in regions where the majority of the hinterland geology is composed of sedimentary rocks. In Morocco (see recent review of the geographical origin of the age populations of the zircons in Lovell-Kennedy et al., 2023), the majority of zircons found in previous detrital studies have been of Pan-African age (0.8–0.54 Ga) (Abati et al., 2010; Domènech et al., 2018), with Eburnean-aged grains forming a significant secondary population (Azdimousa et al., 2019; Marzoli et al., 2017). Alongside these major populations, Leonian-Liberian (3.5–3.0 Ga) and Neoarchean grains (2.5 Ga), corresponding to an unknown tectono-thermal (UTT) event in the WAC (Abati et al., 2010), are a common accessory population. All these populations indicate that the ultimate source for these sediments was the WAC (Abati et al., 2010; Avigad et al., 2012; Gärtner et al., 2017).

The detrital record of Morocco also includes zircon populations which span the Mesoproterozoic (1.6–1.0 Ga) (Accotto et al., 2019; Azdimousa et al., 2019; Ghienne et al., 2018), despite there being no known basement rocks in the WAC that could act as a source for zircons of this age range. Several sources have been proposed for these grains, including the Amazonian Craton Sunsás Belt (Perez et al., 2019), the Taoudeni Basin (Azdimousa et al., 2019; Gärtner et al., 2018), the Arabian-Nubian Shield or Sahara-Meta Craton (Accotto et al., 2019; Marzoli et al., 2017), or hitherto unknown Mesoproterozoic basement in NW Africa (Ghienne et al., 2018). These Mesoproterozoic zircons first appear in the Middle Cambrian (Avigad et al., 2012), becoming up to 30% of the zircons found within Hirnantian glacial deposits (Ghienne et al., 2018). They then diminish to form a significant accessory population during the upper Palaeozoic (Accotto et al., 2019) and the Mesozoic and Cenozoic (Azdimousa et al., 2019).

From Permian times onwards, Variscan grains also form an accessory population indicating that the Meseta and MAM were also a sediment source during the Mesozoic and Cenozoic (Perez et al., 2019). The dominance of Pan-African and Eburnean aged grains within the detrital record makes distinguishing between sedimentary sources difficult, however some trends can be identified.

1. Samples with no Mesoproterozoic populations are likely to have been sourced from WAC basement or Cambrian or older sediments.
2. Samples with Mesoproterozoic populations, but no Carboniferous to Permian grains, are likely to have been sourced from the WAC basement or Cambrian and younger sediment.
3. Samples with Carboniferous to Permian populations must be sourced from either the Moroccan Meseta basement or from Permian to recent sediments.
4. Samples with both Mesoproterozoic and Carboniferous to Permian populations indicate sediment sourced from Palaeozoic sediments, the Meseta basement and/or Mesozoic to recent sediments.

3. Material and methods

In the present study, twelve outcrops where fluvial channels of the Bouzergoun Formation (correlating with the Barremian-Aptian maximum regression), identified by previous studies (Luber, 2017; Luber et al., 2019; Nouidar and Chellai, 2000), were targeted for sampling across the basin. Outcrops coordinates are provided in Table 3 Sedimentary logs are provided on Figs. 16, 17 and 18 in appendices along with the samples' positions within each section. For details of lithology, sedimentary structures, fossil content, biostratigraphy and depositional environments, see Luber (2017) and references therein. Petrography and geochemical analysis were carried out on all samples (Fig. 4).

To be able to compare and detect provenance and spatial variation within the basin, the outcrop dataset was placed into five groups based on geographical location: Tiskatine group (Tiskatine and Assaka sections, northern part of the basin), Tinkert group (Tinkert and Aziar sections, easternmost and most inland part of the basin), Barrage group (Barrage and Akerkaou sections, central part of the basin), Tamri group (Tamri and Mahmout sections, westernmost and most distal part of the basin) and Aouerga group (Addar, Aouerga and Tamzergout, southern part of the basin).

Thin sections were made from all sampled outcrops, they were stained for porosity and calcite and studied using optical microscopy, QEMSCAN and SEM. Thin sections were point-counted (300 points) using the Gazzi-Dickinson method (Ingersoll et al., 1984) and studied for rock fragment populations.

K-Feldspar selective staining using Sodium Cobaltinitrite (SCN), a yellow coloured salt reagent for potassium and ammonium (Bailey and Stevens, 1960), was also applied to quantify the abundance of K-Feldspar (Fig. 5). However, SCN reacted with several minerals and rock fragments, which did not display polysynthetic or Carlsbad twinning, nor showed the crystal morphologies of common feldspars. Thus, additional techniques were used to determine the mineralogical composition.

To help identify the different clasts populations and the nature of the sandstones, QEMSCAN (SEM based automatic mineral mapping) analysis was carried out on samples from each of the outcrops except for those from the Tamzergout and Assaka groups, which were sampled at a later stage. Cell size was set to 20 μm.

3.1. Heavy mineral content

Samples were crushed using a jaw crusher. To minimize the number of broken grains, jaws were brought closer stepwise starting at a spacing of 2 cm. Between each step, the product was sieved at 1 mm and only the coarser fraction was re-crushed.

Samples were dry sieved at 250 μm and wet sieved at 30 μm. Six grams of crushed and sieved (30–250 μm) samples were agitated in 25 ml test tubes with 20 ml of lithium heteropolytungstate (LST, density 2.86 g/cm3). Samples were left for decantation for 3 h after which the bottom centimetre of each tube was frozen using liquid nitrogen. The bottom centimetre (heavy fraction) was recovered, mounted on glass slides, and imaged using QEMSCAN. Identified grains were then individually counted manually from the QEMSCAN maps. The QEMSCAN is unable to identified polymorphs of grains. Therefore, differentiating anatase and rutile could not be done, and both are presented together as titanium oxides.

3.2. Laser ablation U–Pb analysis of zircon

Five outcrops throughout the basin were selected for detrital zircon U–Pb analysis (see symbology in Fig. 4). For each, samples were crushed and sieved at 30–500 μm. Heavy minerals were concentrated using a shaking table and magnetic minerals were removed using a Frantz magnetic separator. Eventually, zircons were concentrated using diiodomethane (3.3 g/cm3) and concentrates were hand-picked, mounted in epoxy disks, polished, and imaged using cathodoluminescence to select laser spots. The separation, mounting and analysis of the zircon grains was conducted at the British Geological Survey (NERC Isotope

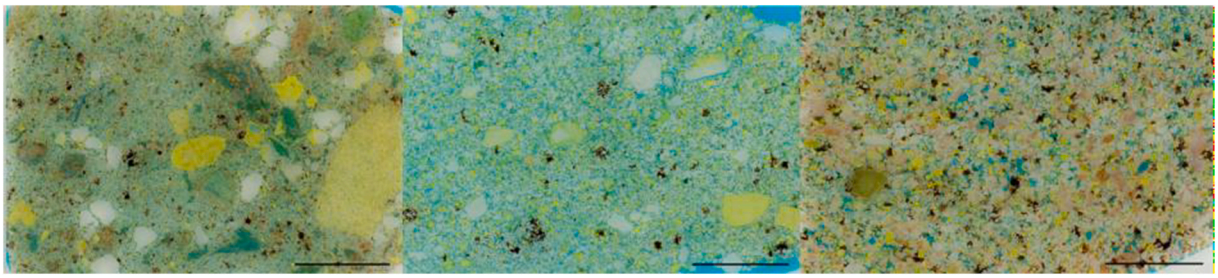

Fig. 5. Thin section overview photographs of MTDAN 863, MTMH722 and MTTM811 (from left to right), where K-feldspar could not be clearly identified. The porosity in observable in blue, the SCN staining visible in yellow, and calcite is characterised by a reddish/pink colour.

Geosciences Laboratories, Keyworth). U–Pb analyses were carried out using a multi-collector Nu Plasma HR mass spectrometer with a New Wave 193 S S solid state laser, typically using a 20–25 μm laser spot, and fluence of c. 2 J/cm^2. Laser spots were selected on core and rim of grains (though the latter were rarer) depending on the pristineness of the grain. Three standards (Plešovice zircon (Sláma et al., 2008), 91 500 (Wiedenbeck et al., 1995), and GJ-1 (^{206}Pb/^{238}U 602.3 ± 1 Ma, ^{207}Pb/^{206}Pb 609.2 ± 0.7 Ma; in-house ID-TIMS) were regularly analysed to correct the instrument mass bias and depth dependent inter-element fractionation of U and Pb. The 91 500 standard was used as primary throughout, yielding a weighted average ^{206}Pb/^{238}U age of 1063.9 ± 2.13 Ma (n = 108). Secondary standards Plešovice and GJ-1 gave weighted average ^{206}Pb/^{238}U ages of 338.3 ± 1.0 Ma (n = 79) and 602.9 ± 1.9 Ma (n = 107) respectively. Data was reduced using Iolite (Paton et al., 2010, 2011) and plotted using IsoplotR (Vermeesch, 2018).

For grains >1200 Ma in age, ^{207}Pb/^{206}Pb ages were used, with a discordance limit of ±10%. For grains <1200 Ma, ^{206}Pb/^{238}U ages were used, with a discordance limit of ±5%. Data tables and interpretations are supplied as supplementary data.

3.3. Low-temperature thermochronology (LTT)

The temperature history of the hinterland source areas was ascertained from published Low-Temperature Thermochronology (LTT). Increasing temperature in a samples thermal history is associated with burial (i.e., sedimentation above the sampled rock) and decreasing temperature with exhumation (i.e., erosion of overburden; Fig. 6). Using depth converted temperature paths, the nature of the surface geology can thus be modelled. LTT datasets often record periods of sedimentation followed by periods of erosion during which the overburden

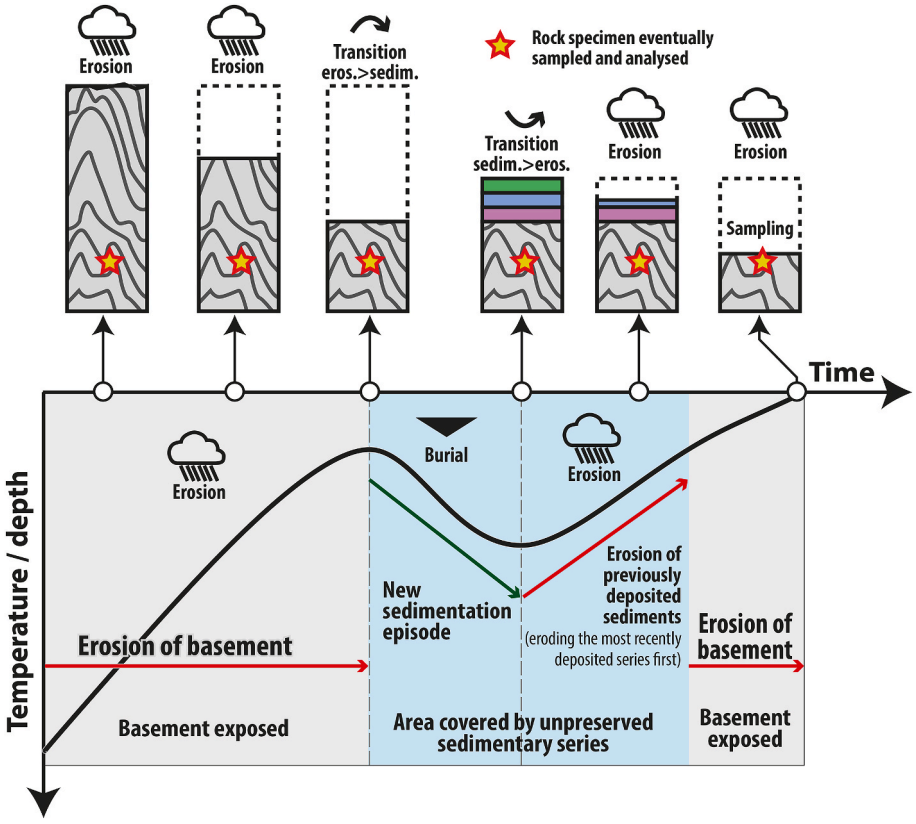

Fig. 6. Exhumation and burial history of a rock sample: temperature paths can be converted to depth if (1) the temperature history is only related to erosional exhumation/burial and if (2) a consistent geothermal gradient was setup in the region. Star = rock sample eventually analysed. In this example, a subsidence/erosion cycle is marked with a blue background. During this event, sedimentation is recorded and followed by subsequent erosion. Once all the previously deposited strata are eroded, basement erosion resumes. The ephemeral sedimentary overburden deposited during this cycle is absent from the modern geology. During the period covered by the subsidence/uplift cycle (blue background), the studied region is covered by sediments which was subsequently eroded, a source of sediment delivered to the basin.

recently deposited is eroded.

This is illustrated by the example presented in Fig. 6, where following initial basement uplift, we can observe a sedimentation/subsequent erosion cycle (the area of the graph with a blue background). During the first part of the cycle, sediments are deposited on top of basement rocks. When the region starts experiencing denudation again, those sediments are gradually eroded, those deposited the latest being eroded first. Once the overburden is completely eroded, basement erosion resumes. The "ephemeral" overburden is not preserved in the modern geological record and can only be identified and reconstructed using the thermal history. Constraining these ephemeral overburden units is critical, as a source region would, during such a cycle, be mostly or entirely absent from the modern day known regional rock record.

Sixteen time-temperature models (references provided in a table of the appendices) were compiled, and the slope gradient of each model was calculated at 125 Ma (Barremian-Aptian transition) and displayed on the regional map (Fig. 7). Each point displays the behaviour (exhumation or burial) of the temperature path during the interval of interest.

Compiling all available LTT data allows for the location of domains undergoing erosion or sedimentation during the Barremian-Aptian transition (125 Ma). Thermochronology data is by nature subject to large margins of error due to a modelling process based on a limited number of constraint points. While those error margins preclude precise time interval interpretations of single data-points, clusters of consistent data points add confidence that observations reflect a regional behaviour.

The depth-converted dataset shown later in the main text was produced using the adaptive geothermal gradient calculated in Charton et al. (2021a) for the different regions and tectonic regimes of Northern Morocco, with a fixed surface temperature of 20 °C. An average gradient of 29 °C/km was chosen for the Variscan orogeny based on available research on the Alps and of 34 °C for the High Atlas based on works carried out in the Rio Grande Rift and in the East African Rift system. A gradient of 27 °C/km was chosen for the High Atlas rift flanks based on values obtained in the East African Rift flanks. Finally, a gradient of 24 °C was applied for the "mature passive margin" and "intra-continental domain" based on previous studies carried out in Morocco. For details and references, see Charton et al. (2021a).

4. Results

4.1. Hinterland analysis

Thermochronology analysis conducted in the hinterland region (see Charton, 2018 for a summary) was reviewed and incorporated into this study. Charton (2018) highlighted that all but two of the time-temperature studies compiled in his meta-analysis recorded Mesozoic erosional exhumation or burial. The only observed exceptions where samples from the Toubkal Massif, where recent tectonic exhumation was the preferred scenario (Ghorbal, 2009) and samples from the Canaries where episodes of regional heating, likely associated with the island formation volcanism, reset the fission track ages (Wipf et al., 2010). This view is consistent with other previous studies which highlighted (1) that magmatic intrusions like the CAMP dykes in the Anti-Atlas did not reset LTT ages in their vicinity (Oukassou et al., 2013) and (2) that thermal subsidence following rifting did not affect the

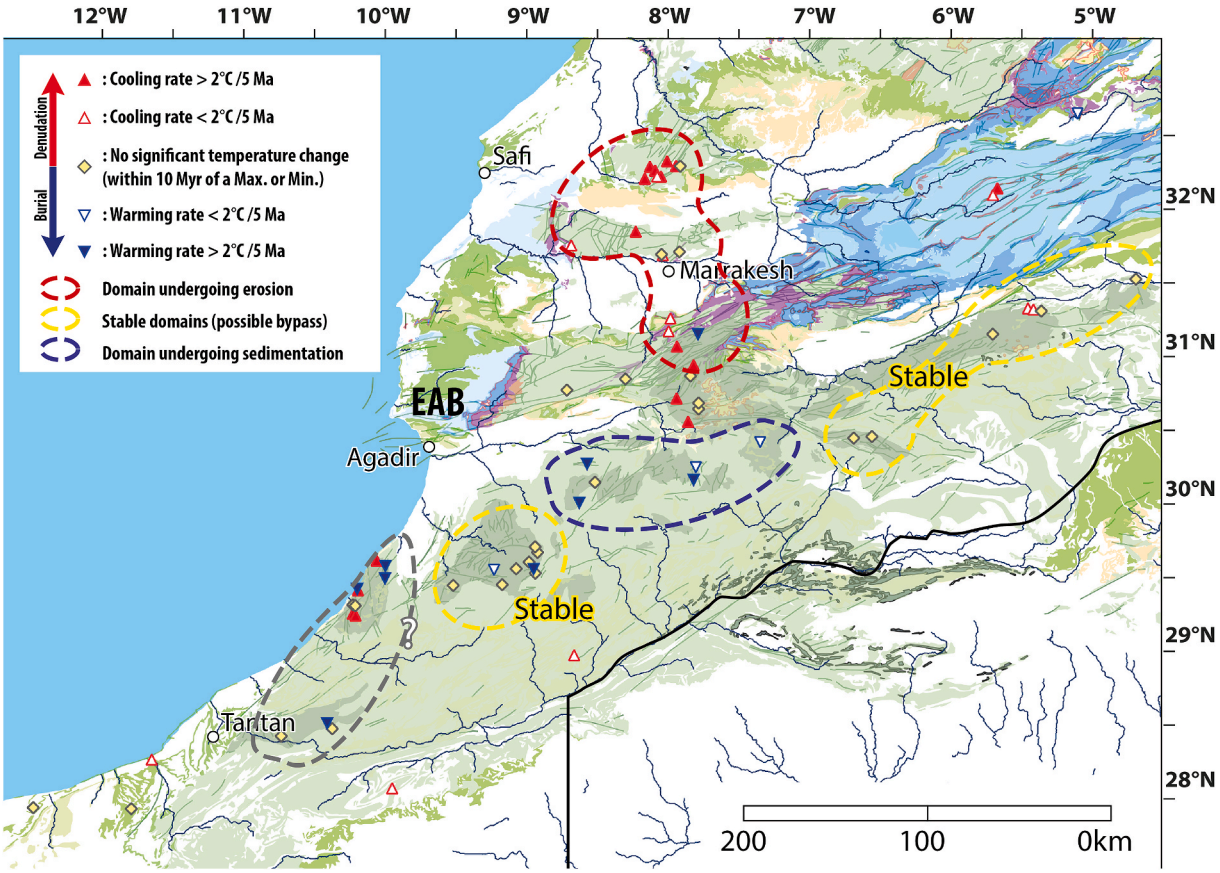

Fig. 7. Temperature evolution gradient of the hinterland of the EAB at 125 Ma. The low temperature thermochronology dataset was assessed as recording erosional denudation (filtered dataset was compiled from: Sabil, 1995; Barbero et al., 2007; Malusà et al., 2007; Ghorbal et al., 2008; Balestrieri et al., 2009; Saddiqi et al., 2009; Ghorbal, 2009; Barbero et al., 2011; Sebti, 2011; Ruiz et al., 2011; Oukassou et al., 2013; Sehrt, 2014; Domenech, 2015; Gouiza et al., 2017; Charton et al., 2018; Leprêtre et al., 2018; Lanari et al., 2020). Areas recording a decrease in temperature (inside red dashed line, demoted by red triangles) are undergoing exhumation (erosion/denudation) while increase of temperature highlights burial (sedimentation) (inside blue dashed line, demoted by blue triangles).

unstretched continental crust adjacent to rift zone/rifted margins (negligible thermal relaxation) (Gallagher et al., 1998).

The behaviour of each LTT temperature path at 125 Ma is displayed in Fig. 7. Compiled LTT datasets for the Barremian-Aptian transition show (1) a homogeneous cluster of data points recording denudation in the Western Meseta and MAM, (2) stable domains around the Kerdous inlier and Eastern Anti-Atlas and (3) burial in the central Anti-Atlas (Fig. 7). Data within the Siroua region (South of the MAM) show a mix of stable and exhuming patterns. Within the Western Anti-Atlas the signal is unclear (Fig. 7), suggesting a transition period between exhumation and burial.

4.2. Petrographic analysis

All studied sections displayed litho-quartzose (7 out of 11 sections) or litho-feldspatho-quartzose, feldspatho-litho-quartzose or quartzo-lithic (4 out of 11) framework composition (see ternary diagram in Fig. 8 based on Garzanti, 2019). Samples throughout the basin display similar rock fragment populations derived from very heterogeneous source terranes (Figs. 9 and 10). Grain size was highly variable, between and within samples, ranging from granule to fine sand. Between 9% and 29% of the point-counted samples comprise intergranular porosity which may be completely cemented by calcite (e.g., Tiskatine, Addar), partially cemented (e.g., Tamri, Mahmout) or free from cement, with visual porosities of up to 21% (e.g., Tinkert, Aziar South). Mono- and polycrystalline quartz make up 31%–55% of the mineralogical content. Grains are angular to sub-rounded, the sub-rounded population being dominant. Calcite precipitation is apparent around some of the biggest rock fragments. Detrital and diagenetic iron oxide and hydroxide grains are usually present and account of up to 6% of the QEMSCAN mineral count (volumetric %), mostly consisting of goethite and hematite. The overall heavy mineral volume was estimated with QEMSCAN to be 0.2 %. QEMSCAN identified most unknown SCN-stained rock fragment as composite grains of clay, quartz, and K-feldspar. Most of these grains displayed no specific features to allow definite identification. They were included within the "rock fragment (unknown nature)" category on Fig. 10.

Throughout the basin a significant proportion of the clasts are derived from volcanic rocks (Fig. 10). It includes populations of pumice clasts (Fig. 9D), embayed quartz, formed in igneous extrusive volcanism events and fragments displaying graphic/granophyric texture. Such intergrowth of quartz and alkali feldspar is commonly found in volcanic clasts (e.g., ignimbrite) or shallow level felsic intrusions (Ulmer-Scholle et al., 2015). Most of these clasts were in an advanced state of weathering and gave similar QEMSCAN signature as unidentifiable SCN-stained rock fragments. Unaltered volcanic glass is known to be isotropic but alteration to quartz or K-feldspar and SCN staining has previously been suggested to help identify the presence of what was once volcanic glass within lava, ignimbrite, or pumice grains (Ulmer-Scholle et al., 2015). As volcanic grains tend to be hard to identify after weathering, as they alter to clays (smectite, illite, chlorite, etc.) (Aomine and Wada, 1962; Sudo, 1954), their original abundance is thought to be larger than that assessed by point-counting (Fig. 10) and was possibly an important part of the unidentified SCN-stained grains.

All samples were poor in feldspar (4.2% in average, see QFL on Fig. 8). Grains identified as feldspar were in an advanced state of alteration and commonly reacted with SCN staining. Some clasts remained identifiable by displaying characteristic white perthitic worm-like structures, interpreted as albite exsolution lamellae (Fig. 9C). The SCN-stained part of the grain in Fig. 9C is likely made of K-feldspar partially altered to albite and clay minerals. Pores likely formed during the weathering process and were filled by calcite or quartz cement (≈50 μm roundish/elongated structures visible in the grain). The preferential dissolution of the albite lamellae may create important porosity, up to 10% in the grain displayed in Fig. 9C, speeding up weathering of the grain. Dissolution is likely to have been prominent after deposition as the observed degree of dissolution of perthite grains is incompatible with transport (Fig. 9A).

All samples display an important (6–16%) population of volcanic-derived rock fragments (Figs. 8, 9D and 9E, and 10). Carbonate rock fragments/calcareous clasts are also consistently present throughout the basin (see proportion on Fig. 10; e.g., Jaillard et al., 2019a), especially in the Tamri group. This group is dominated by rounded to subrounded clasts of calcite, with rare, rounded fragment of fossil bearing limestone also present (e.g., possible serpulids; Fig. 9B). Rare grains of quartz displayed vermicular chlorite inclusions (Fig. 9F), typically derived from terranes subject to hydrothermal alteration (Espejo and Lopez-Gamundi, 1994) or within metamorphic or pegmatitic terrains (Ulmer-Scholle et al., 2015). Metamorphic-derived rock fragments were found throughout the basin and stratigraphy, except during deposition of the Tamri group. All sample groups have polycrystalline quartz, differentiated based on the shape of quartz minerals within the clast as plutonic and detrital origin. When the distinction between either category was unclear, grains were simply identified as polycrystalline quartz ("Qtz – Poly" on Fig. 10).

4.3. Detrital zircon dating

All samples display the characteristic northern WAC detrital zircon spectrums dominated by a major peak of Pan-African age and a secondary peak of Eburnean age (Fig. 10). The Tiskatine group (north) have the most diverse assemblage of secondary populations including

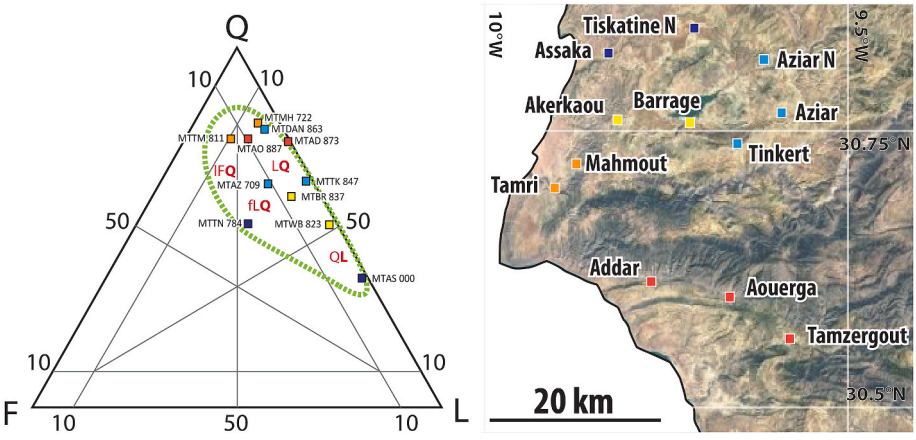

Fig. 8. Sampled outcrops with analysis conducted and QFL diagram of point-counted samples (layout after Garzanti, 2019); orange = Tamri group, yellow = Barrage group, dark blue = Tiskatine group, light blue = Tinkert group, red = Aouerga group.

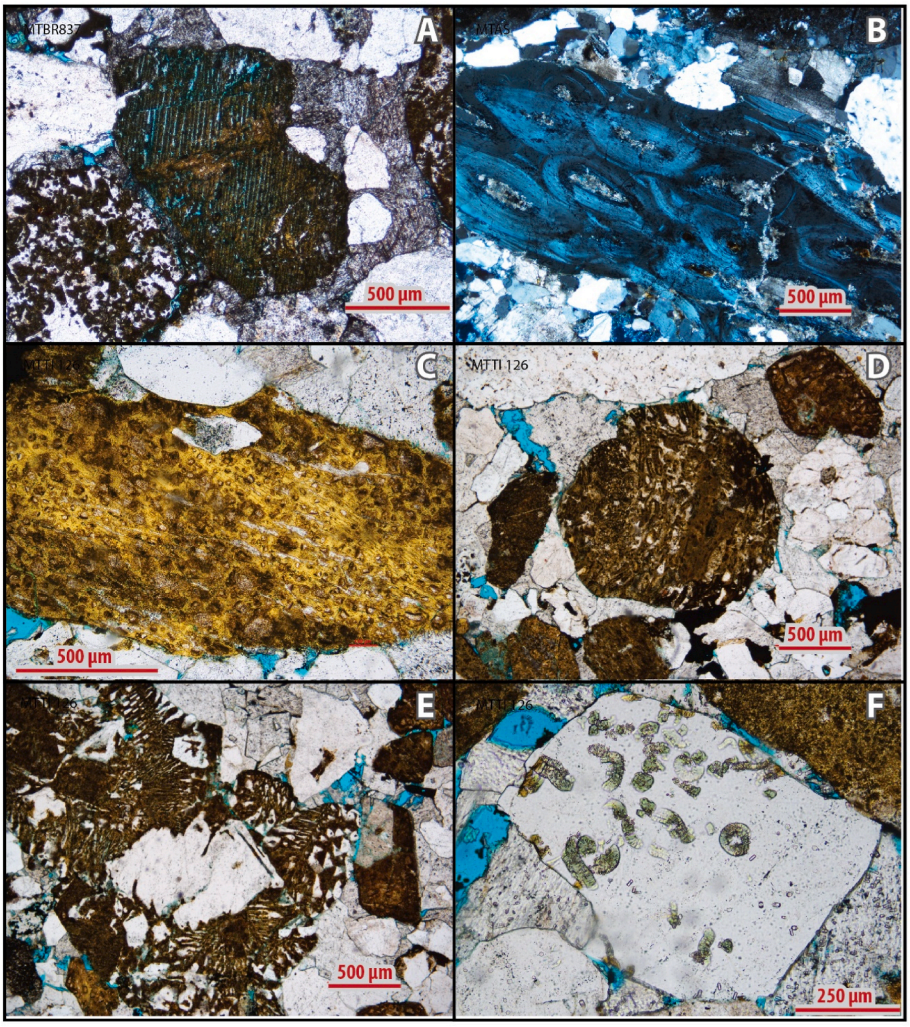

Fig. 9. Microphotographs (polarised light) of clast populations: A: Perthite grain with dissolved albite lamellae, this level of dissolution is incompatible with transport and likely to be post-depositional; B: Deformed possible serpulids or ooids with pore filling carbonate cement; C: deeply weathered feldspar with exsolved albite lamellae and inclusion; D: SCN stained grain of pumice; E: Granophyric texture commonly found in volcanic terranes or shallow felsic intrusion; F: Hydrothermal chlorite inside of a quartz grain (hydrothermal metamorphism).

Variscan grains and Mesoproterozoic grains. Samples from the Aouerga group (south) have similar populations, but a single Variscan grain was also recorded. This Variscan population was not found in the Barrage and Tinkert group. All samples have at least one grain of Mesoarchean age (around 3 Ga) and the Tiskatine group contains the only grain in the dataset of Paleoarchean age. Mesoproterozoic grains were present as a trace population in all samples. Overall, no distinguishing populations or trends are visible between the northern and southern part of the basin.

4.4. Heavy minerals

Heavy mineral assemblages within a sedimentary rock are the results of various factors: lithology of the parent rocks, weathering in the source area, mechanical abrasion during transport, post-depositional weathering, hydraulic processes, diagenesis, and weathering at outcrop (Guedes et al., 2011). Samples were variably affected by dolomitization and iron oxides and had different heavy mineral yields. In sample MTTN784 from the Tiskatine group, 80–90% of the separated heavy minerals were dolomite fragments (Fig. 11) and only 126 non-dolomitic transparent heavy minerals were present in the mount. In other samples, the number of transparent heavy minerals recovered (excluding iron oxides and dolomites) varied between 222 and 312.

In all samples, the heavy mineral content is dominated by the most stable minerals (titanium oxides, apatite, zircon and tourmaline) (Morton and Hallsworth, 2007), with Zircon-Tourmaline-Rutile (ZTR) ratios (Hubert, 1962) of 75–86%. Titanium oxide minerals largely dominate the heavy mineral mix (65–75% of grains), and all samples present an important population of apatite (5–19%). Rare olivines are also present throughout the basin (0.5–1.8%) (Table 1). The only compositional differences between samples are within trace populations: the Tiskatine group do not have amphibole which accounts for 0.9–1.7% of other groups, nor does it have pyroxenes (0.5–0.7% in other groups) or garnet (0.5–6%). Cr-spinels were only detected in the Tinkert group (4 grains, 0.7% of HM mix). Those differences among populations are represented by very small number of grains (4 or less) and may be the result of statistical effects.

4.5. Offshore sedimentary systems and seismic geometries

2D seismic profiles were recently interpreted to study slope processes and offshore behaviour of the sediment supply (Muniz-Pichel, 2018). We interpreted seismic profiles from a zero-phased time-migrated dataset covering c. 2500 km^2 offshore the Essaouira-Agadir Basin.

Some offshore profiles display lenticular to convex-shaped mini-basins that developed during the Barremian-Aptian, Cenomanian and possibly as early as the Jurassic. They are characterised by often having internal high-amplitude seismic facies (Fig. 12). These structures are

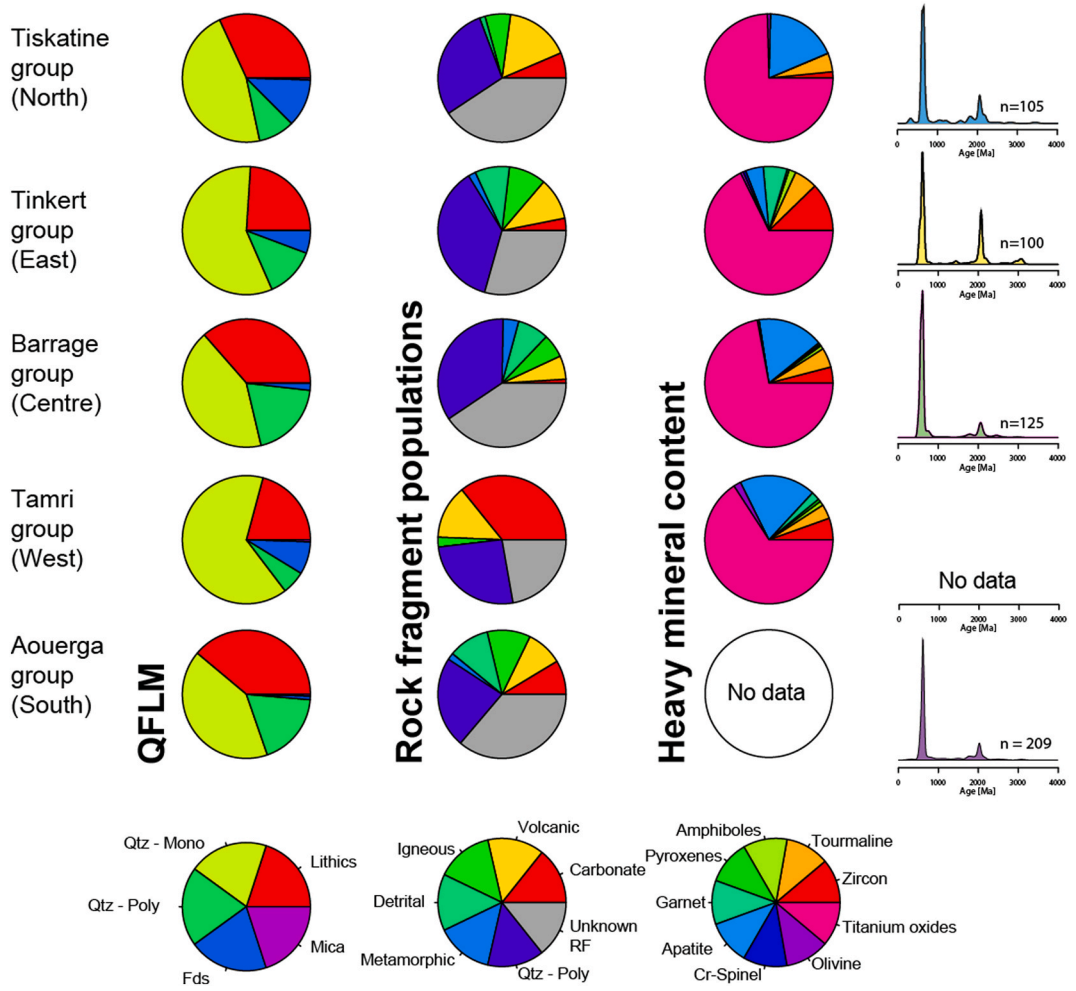

Fig. 10. Modal composition, rock fragment population, heavy mineral content, and detrital zircon spectrum of studied sample groups. In brackets (e.g., North) is the relative position of these groups within the onshore EAB.

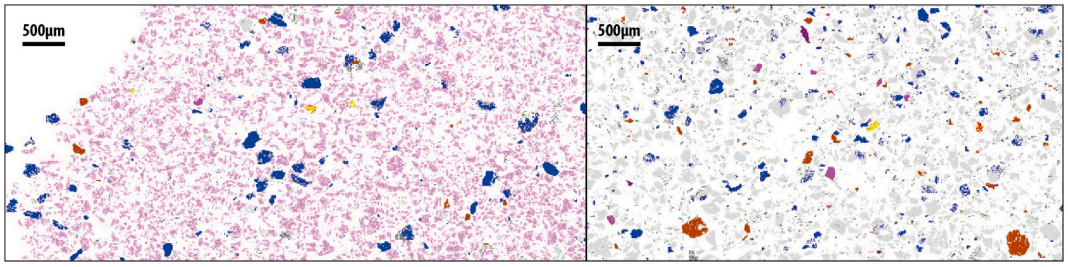

Fig. 11. Overview of heavy mineral mounts from samples MTTN784 and MTTM811, dolomite in light pink and iron oxides in light grey account for most of the signal in each sample (other minerals: apatite in brown, zircon in purple, titanium oxides in blue, tourmaline in yellow).

located withing structural lows and display onlaps towards upturned strata on the flank of diapirs and/or salt-cored anticlines. They can be mapped within the two more proximal mini-basins in the mid-slope, seen on several profiles, indicating a direction of sediment transport towards the NNW, likely due to deflection around NNW-trending diapirs.

5. Discussion

5.1. Barremian-Aptian hinterland denudation and surface geology

Thermochronology data record denudation and burial of the MAM and Western Meseta during the Barremian-Aptian transition (Figs. 7 and 13). Data within the Anti-Atlas do not show any trend of denudation. The vertical movement history of the Western Anti-Atlas is unclear, but the dominance of east-west oriented paleocurrent measurements in the EAB supports a dominant sediment source from the east. This would support the model for no or limited sediment input coming from the Western Anti-Atlas located to the south or south-west. Paleocurrent data does not allow discrimination between the MAM and Western Meseta source areas.

Low-temperature thermochronology data and depth-converted time-temperature modelling results in the MAM and Western Meseta (Domenech, 2015; Charton et al., 2021a) indicates the presence of unpreserved overburden, covering both regions during the Barremian-Aptian transition (Fig. 13). At that time, both regions were at

Table 1
Result of heavy mineral point counting. Conducted on QEMSCAN maps of mounted heavy mineral condensates.

	Tinkert-Aziar group (East)	Tiskatine Assaka group (North)	Tamri-Mahmoud group (West)	Barrage-Akerkaou group (Centre)
Zircon	71	2	15	9
Tourmaline	34	6	10	11
Amphibole	10	0	3	2
Pyroxene	3	0	2	1
Garnet	35	0	6	1
Apatite	26	23	53	37
Cr-Spinel	4	0	0	0
Olivine	4	1	5	1
TiO2	392	94	181	160

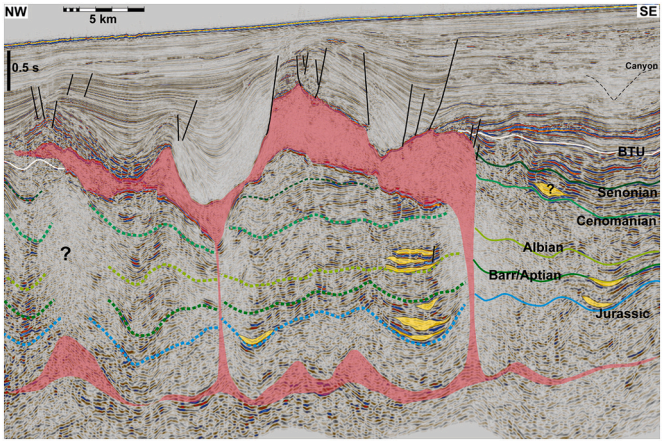

Fig. 12. Interpreted seismic profile trending SE to NW (offshore Assaka, see location on Fig. 1. Salt canopy in red, high amplitude channel-like possible sand bodies in yellow. Uninterpreted version provided in appendices. BTU = Base Tertiary Unconformity.

the end of a burial/exhumation cycle, during which Permian, Triassic and Jurassic sediments that had been deposited above the Palaeozoic and Precambrian basement, were later eroded following uplift. This sediment cover over the Western Meseta was originally deposited when the region underwent burial during the Permian, Triassic to Early Jurassic time (Fig. 13). LTT data suggests the region recorded the accumulation of 2.5–4 km of sediment before exhumation resumed around 180 Ma ago.

Between the onset of the exhumation phase and the Barremian-Aptian transition, a large part of this overburden was eroded. The Western Meseta is modelled to have been covered by up to 1 km of uppermost Permian (in the Jebilets) to Triassic sediments, which would have been eroding and a source of sediment. It is likely the Jurassic sediments would have already been eroded by this time. It is possible that erosion could have already extended down to the basement in the Rehamna massif.

This suggests the dominant eroding lithologies within the overburden during the Barremian-Aptian were likely dominated by Triassic conglomerate and sandstones (Mader et al., 2017; Medina, 1995) and Permian continental clastic deposits, as described from preserved stratigraphy described by Hoepffner et al. (2005).

The MAM also underwent burial during the Late Triassic and throughout the Jurassic before exhumation resumed around the Jurassic-Cretaceous boundary (Domènech et al., 2016). In total, 3–4 km of sediment may have been deposited over the MAM Palaeozoic/Basement (see Fig. 13 at ~200-150 Ma). Part of it was subsequently eroded and during the studied interval, the MAM is modelled to have been covered by a Late Triassic-Middle Jurassic overburden with a thickness from a few hundred metres to up to 1.6 km (c.f., ~125 Ma; Fig. 13).

5.2. *Nature of unpreserved overburden*

Depth converted subsidence curves indicate a 2–4 km thick overburden over the Rehamna, which was mostly or entirely eroded by the Barremian-Aptian, likely resulting in basement exposure. In the MAM, at least ~2 km of Triassic to Middle Jurassic sediments covered the basement terranes (Charton et al., 2021a), and perhaps up to 4 km, as documented by the ZHe results from Domènech et al. (2018).

In the Lower to Upper Triassic, sedimentation within the MAM is thought to be dominated by siliciclastic deposits (both sandstones and mudstones). This interpretation is based on remnants of Permo-Triassic sediments preserved in intra montane rift basins (Fabuel-Perez et al., 2009; Le Roy and Piqué, 2001) (e.g., Oukaimeden basin, Tizi N Test basin) and paleogeographic reconstructions (Beauchamp, 1988; Frizon de Lamotte et al., 2008; Medina, 1995). Frizon de Lamotte et al. (2008) also predict the sedimentation of unpreserved conglomerate and clastics in the Western Meseta, although no remnants are preserved to test this model. Those Triassic continental clastics would have transitioned laterally towards the west into an alternation of siltstones and sandstones as visible in the DA8 well (Doukkala basin, Le Roy and Piqué, 2001), and be capped by evaporites and basalts during the Latest Triassic/Sinemurian (Le Roy and Piqué, 2001; Medina, 1991; Sahabi et al., 2004).

During the Triassic-Jurassic transition, extensive tholeiitic flood basalts of the Central-Atlantic magmatic province were also extruded

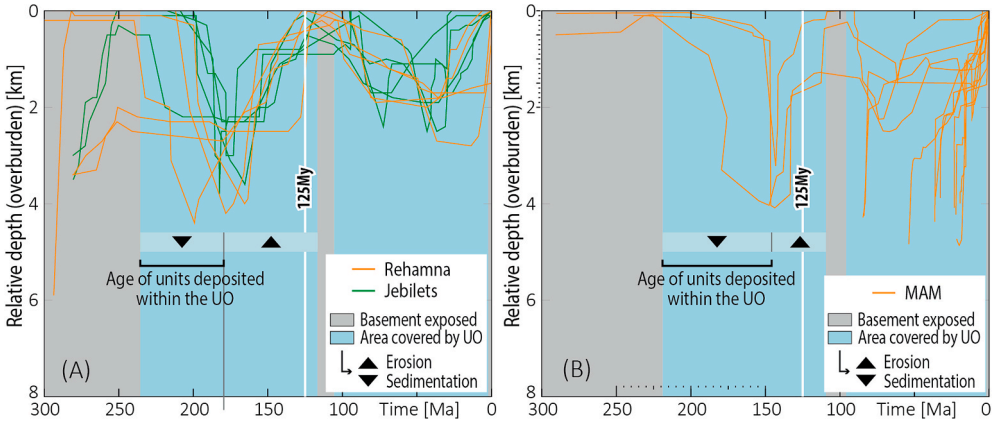

Fig. 13. Depth converted LTT data in the Western Meseta (A) and MAM (B), modified from Charton et al. (2021a). UO = unpreserved overburden; grey background = periods of basement exposure, blue background = burial/exhumation cycle during which the studied region is covered by an overburden absent from the modern geology.

around the MAM region, dated to 200 ± 3 Ma (Schlische et al., 2013). The data shows that the MAM was undergoing burial during the Triassic-Jurassic transition (Fig. 13) and while these rocks are mostly not preserved today, CAMP basalts are expected to have been deposited widely across the MAM region, with a calculated average thickness of 225 ± 75 m based on surrounding regions (150 m thick basalts in the Argana basin (west of the MAM), and 300 m in the Central High Atlas (Le Roy and Piqué, 2001; Marzoli et al., 2019).

These results suggest that during the Barremian-Aptian the surface geology in the Jebilets was likely dominated by Permian-Triassic coarse clastic sandstones and mudstones, covering most or all the Palaeozoic basement. Erosion of these exposed formations across the region is expected to yield good quality sands. The Triassic sandstones in the MAM are modelled to have been partly covered by CAMP volcanics and younger Jurassic lagoonal deposits, which would have delivered a sand-rich but more heterogeneous mix, with basalt, clay, carbonate, and siliciclastic rocks undergoing erosion.

5.3. Intra-basinal homogeneity

The integrated dataset of detrital zircon geochronology, heavy mineral and petrography point toward a similar recycled source for the different parts of the basin.

Eburnean and Pan-African peaks within detrital zircon datasets are common throughout north Africa and are too widespread to be used as a provenance indicator (all possible source terranes are susceptible of yielding such ages). The studied dataset however contains rare Variscan grains recorded in both the Tiskatine group (north of the basin) and Aouerga group (south of the basin) and we submit that they are likely present throughout the basin, suggesting at least one common sedimentary source located to the east. Note that the population was probably not detected within the Tinkert and Barrage groups due to their limited sample size (respectively 100 and 125 grains).

The scarcity of feldspars and the abundance of sub-rounded quartz and sedimentary rock fragments tends to indicate that source terranes are dominantly sedimentary in nature. The low heavy minerals contents estimated using QEMSCAN (0.2 % of the total mineral volume) is consistent with this interpretation and suggests reworking of a mature sediment input. The homogeneously high ZTR ratios in all analysed samples also suggest a very high degree of mineralogical maturity and may be the result of recycling and/or of post-depositional dissolution of less stable mineral species (Garzanti and Andò, 2007).

Heavy mineral contents are similar between samples throughout the basin with minor differences in the east (Tinkert group), which has higher proportions of zircon, tourmaline, amphibole, garnet and is the only sample containing Cr-spinel. However, the sample also has the lowest apatite content (4.5% versus 17–19% in other groups). Apatite is known to break down easily when exposed to weathering (Morton, 2012) and the higher values of secondary populations observed in the Tinkert group are likely a statistical effect due to the loss of apatite crystals during the post-depositional weathering, increasing the relative proportions of other mineral populations.

The nature and proportion of rock fragment populations is also similar throughout the basin with important carbonate, volcanic, detrital, and plutonic lithic fragment. The Tamri area is the depocenter of the Late Barremian sandstones and constitutes the river mouth of a river that originates in the Imi'n'Tanout area, (i.e. between the MAM and Jebilets massifs; Jaillard et al., 2019a). The Tamri group is enriched in carbonate rock fragment and has reduced detrital and plutonic rock lithic content relatively to other populations. However, the group is surrounded to the north, east and south by sections sharing a high degree of similarity, and the peculiar fingerprint of the Tamri group is unlikely to be the result of a different regional provenance, but more likely the result of local sediment sources (possibly from the Cap Ghir paleohigh) or the result of hydraulic sorting.

5.4. Provenance correlations

Samples throughout the basin contain Variscan grains only known to be sourced from Variscan plutonic units or Permian and Triassic detrital terranes of the Western Meseta and MAM.

Based on the expected lithologies within the unpreserved overburdens, Permian and Triassic sediments are the most likely source of most of the clastics to the EAB. Triassic sediments of the MAM and Argana Valley (Eastern EAB) are characterised by the presence of Variscan-aged grains and a minor but consistent Mesoproterozoic population. Archean grains can represent a minor population, as exemplified in Marzoli et al. (2017), Perez et al. (2019) and Domènech et al. (2018). At the same time, they have been documented as a major population observed in the Upper Triassic in Oukaimeden and Tizi N'Test (Perez et al., 2019; Domènech et al., 2018).

Samples from the Barremian-Aptian in the EAB (Fig. 14) contain grains within all these expected age windows and have a relative scarcity of Archean ages. The proportion of dominant and accessory zircon populations correlate with sediment supplied at least in part from reworked Triassic sediments.

The MAM is the best candidate for the pyroxene/olivine content and volcanic lithics, likely derived from the erosion of CAMP basalts, expected at the time to have covered this region. While the Western Meseta is also thought to have been subsiding during the Triassic-Jurassic transition and therefore possibly had CAMP volcanics, the LTT data indicate those would have been eroded before the Barremian-Aptian transition (Fig. 13).

During the studied interval, the MAM is also modelled to have been covered by a sedimentary overburden comprising of limestones and sandstones, making it the only known match for the observed rock fragment populations recorded from the basin.

The origin of the apatite crystals is uncertain. Apatite is present in our dataset in greater proportion than zircon and tourmaline. While it is among the most stable heavy minerals (Morton and Hallsworth, 2007), it remains more fragile than zircon, tourmaline and rutile. Two origins can be proposed. Apatite crystals can be recycled and are very resistant to transport and diagenesis when preserved from acidic weather conditions (O'Sullivan et al., 2020). They have been documented surviving billions of years (Kenny et al., 2019) and are commonly found in larger proportions than zircon in both igneous (Kenny et al., 2019) and metamorphic rocks (Spear and Pyle, 2002). Therefore, the most likely source is recycling of apatite crystals through the Triassic and Jurassic overburden covering the MAM, due to its exhumation during the Late Barremian, and thus potentially Early Cretaceous to Barrremian deposits/intrusive rocks (e.g., Couches Rouges interbedded with Barremian basalts present further east in the Central High Atlas, which underly and are covered by fluvial units, Bensalah et al., 2013; Michard et al., 2013). This would imply that the region was not subjected to acidic weathering during its erosion, that the original source rock (Triassic-Jurassic sediments) had a rich apatite content, and that the sediment underwent a limited amount of recycling events.

An alternative option would be the direct contribution during the Barremian-Aptian of a source of sediment of igneous or metamorphic nature. No obvious candidates are present in the hinterland, however, the existence of the Toubkal horst has been proposed by previous authors and the exposure of Precambrian terranes (likely granites) around the Toubkal massif is possible (Bertotti and Gouiza, 2012; Domènech et al., 2016). The first hypothesis (a recycled signal) is preferred, as the limited exposure and known poor apatite content of the Precambrian massifs of the MAM does not make them a suitable candidate (Missenard et al., 2008). The homogeneous fingerprints throughout the basin suggest all sections are being sourced from similar terranes, and the petrographic dataset points toward sediment supplied in part or entirely from the MAM through an *E*-W local drainage. If the presence of *E*-W rivers flowing from the MAM into the EAB and to the coast is accepted, a transport route for Mesetian sediments to reach the southern part of the

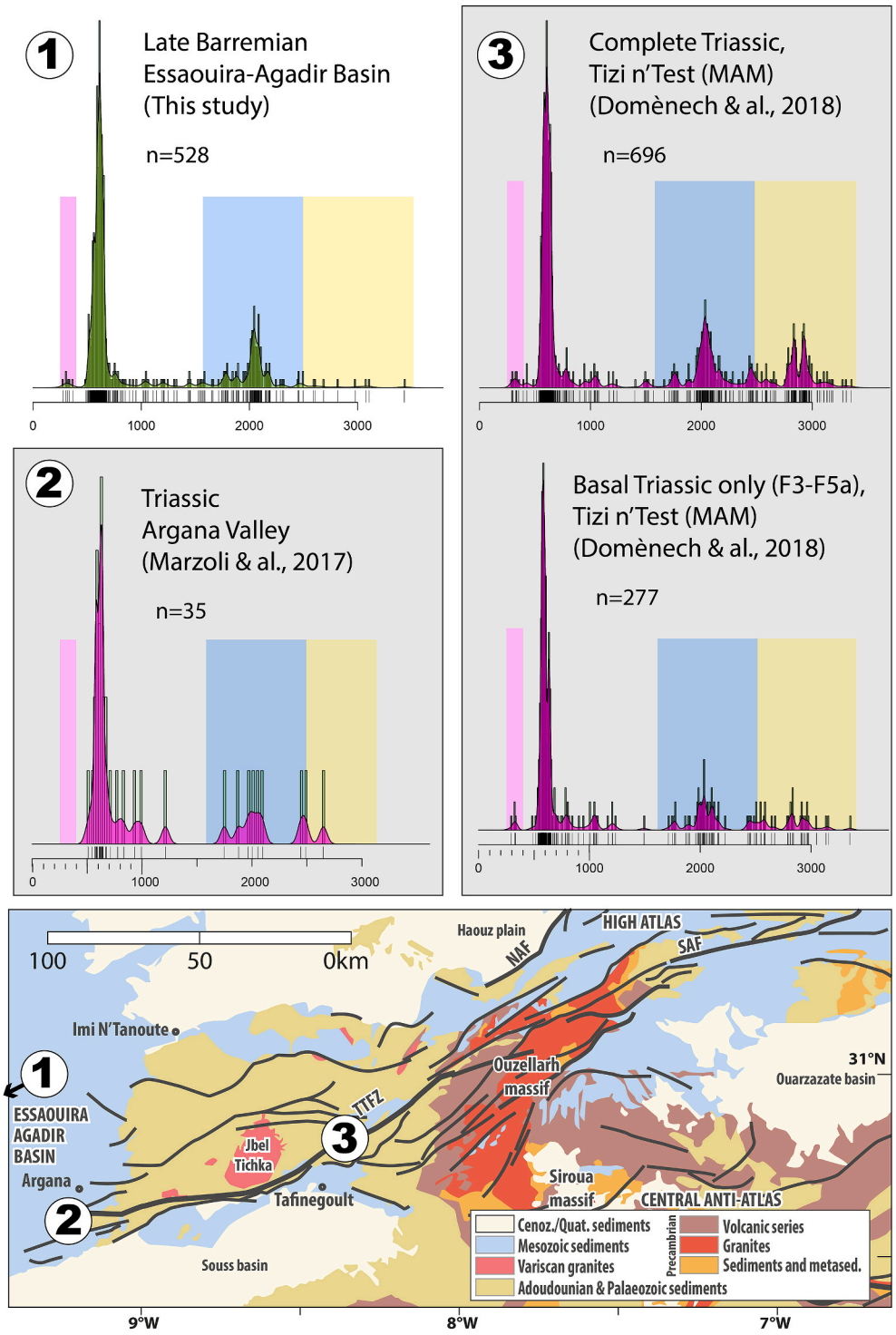

Fig. 14. Similarities between detrital zircon geochronology data from Triassic and Late Barremian sediments (Domènech et al., 2018; Marzoli et al., 2017). Colour bands: pink = Variscan, blue = Paleoproterozoic, yellow = Archean.

basin would involve paths perpendicular and across those rivers, which does not best fit with a realistic scenario. The Western Meseta (especially the Jebilets massif) is expected to yield sand rich sediment during the studied interval and a significant clastic influx to the north of the basin would have affected the fingerprints observed in the Tiskatine group.

Comparison of these detrital zircon results from the EAB with a sample by Perez et al. (2019; sample #14MCO in the undifferentiated lower Cretaceous), in the northern High Atlas foothills, shows similar populations, as well as lithologies of clasts (Jaillard et al., 2019a), possibly indicating that large drainage systems coming from the Meseta existed.

All evidence points toward a proximal source, with the MAM as the dominant and possibly exclusive source of sediment of the system.

5.5. *Nature of the sediment supply and offshore component*

The LTT data indicate that the MAM region underwent a burial/exhumation cycle (Fig. 13), culmination in the Barremian/Aptian. The

MAM was likely covered by Permian and Triassic clastics that subsequently underwent erosion. In addition, earlier in the Barremian, CAMP and Jurassic lagoonal deposits supplied the EAB with dissolved carbonate, sands and clays resulting from the weathering of volcanic/basaltic rocks and erosion of Jurassic mudstones.

The Late Barremian was a time of globally falling relative sea level (Haq, 2013; Frau et al., 2020), and this coincided with the Late Barremian forced regression observed here (Luber, 2017; Jaillard et al., 2019a). Falling sea level may have thus allowed the progradation of deltas or clastic dominate shorelines towards the shelf edge (Luber, 2017, Luber et al., this issue). Sedimentary and paleogeographic reconstructions for the two sequences of interest (sequences 4, 5, and 6 in Jaillard et al., 2019) show sand-rich shelf sediments for the west of the study area, with also the possibility of fluvial conglomerates at the very top of the section (Assaka section, Luber, 2017; Luber et al., 2019). Clastic sediments that were supplied to the slope/offshore domain could have been transported further offshore through canyons/deep water channel systems.

Seismic imaging suggests the presence of synchronous deep-water channels in this interval, located in structural lows created following diapiric salt movement (i.e., mini basins; Fig. 12). If synchronous, these channels evidence a slope break close to the present-day shoreline, as suggested also by (1) the strongly condensed sedimentation (superimposed phosphate layers) in the Assaka to Tafadna areas (Luber, 2017; Luber et al., 2019; Jaillard et al., 2019), likely related to upwelling, and (2) the *N*–S trend of isopachs for the latest Barremian deposits (Jaillard et al., 2019a). Sediment transport direction was variable and likely the same as the input direction from the shelf, with sediments probably deflected and ponding behind and around mobile evaporitic structures (e.g., Amsittene and Imouzzer evaporite-cored anticlines; Charton et al., 2021b), with coarser clastic partly trapped within more proximal, mid-slope mini basins. Sedimentological evidence (local, carbonate-rich conglomerates in the Tamzergout area (Fig. 4) also suggests that there was a quartz-rich river north of the Imouzzer anticline, and that the latter structure was submitted to erosion, thus feeding a small southern river transporting carbonate clasts (see Jaillard et al., 2019a). The orientation of sediment transport offshore is speculative due to lack of paleocurrent data. Having been delivered to the west over the slope, intra-basinal currents may have deflected sediment input. An overall NNW drainage direction is expected offshore the northern part of the basin (deflecting around *N*-NW-trending diapirs) while the southern part was not imaged and might have been feeding an early Agadir Canyon (Fig. 15).

Synchronously, the Mesetian domain was likely to be undergoing denudation and shedding a sand-rich sediment supply further north, although we do not have data to constrain this as it was outside of the sampled region. That associated river system is not preserved at outcrop, and the geometries of the onshore drainage pathways are unknown. However, if the offshore NNW deflection of the sediment supply along the northern part of the EAB occurred, mixing between MAM and Mesetian sands would be likely offshore Essaouira.

Our modelled source-to-sink system (Fig. 15) covers a moderate size catchment area of approximately 35 000 km^2. The longest river channels extend approximately 250 km inland. The offshore dataset does not cover the deepwater fan area, which is expected to be east of Essaouira. Previous meta-analysis have highlighted the existence of correlations between defining parameters of source to sink systems; especially between catchment size and gradient, maximum river length and fan dimensions (Helland-Hansen et al., 2016; Sømme et al., 2009). By comparing the size of the model with analogues, several onshore and offshore parameters can be estimated. In systems of similar size, the fan area covers on average a surface of 10 500 km^2 with length of up to 400 km (150 km on average). Based on the catchment size and river length, the main river channel gradient can be estimated to 6 m/km with maximum altitudes in the hinterland of 3000 ± 1000 m.

6. Conclusion

Twelve outcrops of the Essaouira-Agadir Basin exposing shallow marine and fluvial sandstones of the Late Barremian regression were

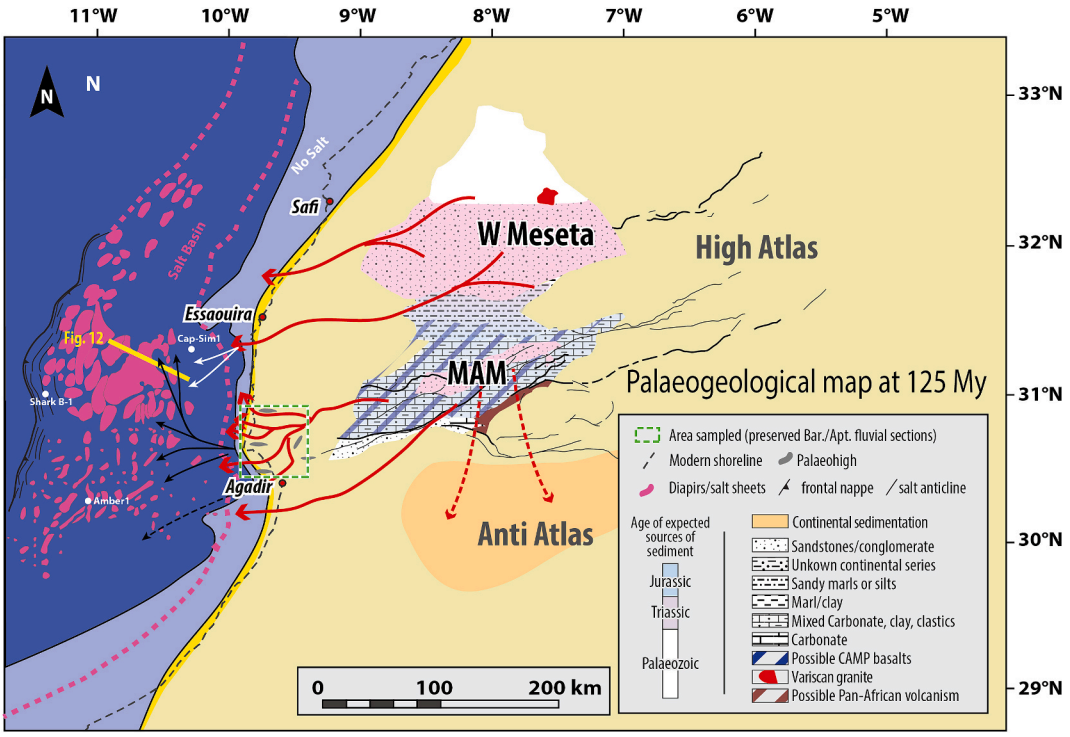

Fig. 15. Source-to-sink model for the EAB and surrounding domains during the Late Barremian, modified after Charton et al. (2021b; and references therein). Onshore drainage marked in red, offshore drainage in black (dashed lines shows lower confidence, see text for details). Rehamna massif displayed here without overburden (basement exposed) as its presence at the surface around 125 Ma is suggested in time-temperature models (e.g., Ghorbal et al., 2008).

sampled and analysed. Thin section petrography and SEM, heavy minerals analysis, and detrital zircon dating were conducted and integrated with a large dataset of published low-temperature thermochronology studies to model the associated source-to-sink system. The homogeneity of fingerprints throughout the basin indicated a single provenance for both the northern and southern studied transects.

The hinterland analysis based on LTT data reveal that only the Western Meseta and MAM regions were possible source candidates for the Late Barremian sediments deposited in the EAB. This is supported by the strong affinity of the detrital zircon geochronology with Triassic sediments modelled to have covered the MAM and parts of the Western Meseta at this time.

LTT data reveals that both regions were at this time covered by Mesozoic sequences overlaying the Palaeozoic basement.

Heavy mineral populations support recycled sediment sources consistent with Triassic/Jurassic sediments and rock fragment populations in the EAB reveal clasts of limestones, sandstones and volcanic nature that can only be correlated with the MAM.

The modelling suggests a source-to-sink system of moderate size (200–300 km long) with an exclusive or dominant source located in the MAM (western High Atlas). This provides the best fit explanation compatible with each dataset examined. This likely provided a sand-rich mix of sediment resulting from the erosion of Triassic continental basins, with associated clays resulting from the weathering of basalts and Triassic/Jurassic mudstones.

The Late Barremian/Aptian eustatic fall in sea level, together with local tectonics, resulted in a forced regression in the EAB at this time, which allowed progradation of the fluvio-deltaic system closer to the shelf edge.

Sediment supply should have been enhanced at this time within the slope/offshore domain.

Seismic imaging suggests the presence of synchronous high reflectivity deep-water channels located in structural lows controlled by diapiric salt movement.

While the southern part was not imaged and might have been feeding an early Agadir Canyon, an overall NNW drainage direction is speculated (based on seismic evidence) for the offshore in the northern part of the basin.

The Mesetian domain is likely to have been undergoing denudation at the same time and shedding a clastic-rich sediment supply north of the studied region.

Mixing between MAM and Mesetian sands is expected offshore Essaouira.

CRediT authorship contribution statement

Emmanuel Roquette: Writing – original draft, Visualization, Validation, Software, Resources, Project administration, Methodology, Investigation, Formal analysis, Data curation, Conceptualization. **James Lovell-Kennedy:** Writing – original draft, Visualization, Validation, Resources, Methodology, Formal analysis. **Leonardo Muniz Pichel:** Writing – review & editing, Visualization, Software, Methodology, Investigation. **Stefan Schröder:** Writing – review & editing, Writing – original draft, Validation, Supervision, Resources, Project administration, Methodology, Investigation, Funding acquisition, Data curation, Conceptualization. **Rémi Charton:** Writing – review & editing, Writing – original draft, Visualization, Validation, Software, Resources, Methodology, Investigation, Data curation. **Ian Millar:** Writing – original draft, Resources, Methodology, Investigation. **Camille Frau:** Writing – review & editing, Validation. **Jonathan Redfern:** Writing – review & editing, Writing – original draft, Visualization, Supervision, Resources, Project administration, Funding acquisition, Data curation, Conceptualization.

Declaration of competing interest

The authors declare that they have no known competing financial interests or personal relationships that could have appeared to influence the work reported in this paper.

Data availability

Data will be made available on request.

Acknowledgments

This study forms part of the lead authors PhD at the University of Manchester with the North Africa Research Group (NARG). The authors would like to thank the sponsoring companies of NARG and the Office National des Hydrocarbures et des Mines (ONHYM) for their continued logistical, field, and scientific support. The constructive comments of Rhodri Jerrett (University of Manchester) and Giovanni Bertotti (TU Delft) are highly appreciated and improved the manuscript. Dr. Stephen Crowley from the University of Liverpool is thanked for giving us access to their crushing/sieving lab while simultaneously guiding us in setting up a separation laboratory in Manchester. BGS Keyworth's facilities and workers are thanked for the picking/mounting/dating of detrital zircons, which was carried out during the second semester of 2018. Finally, we thank the two reviewers (Etienne Jaillard and Antonio Teixell) who significantly improved the manuscript with their comments.

Appendices.

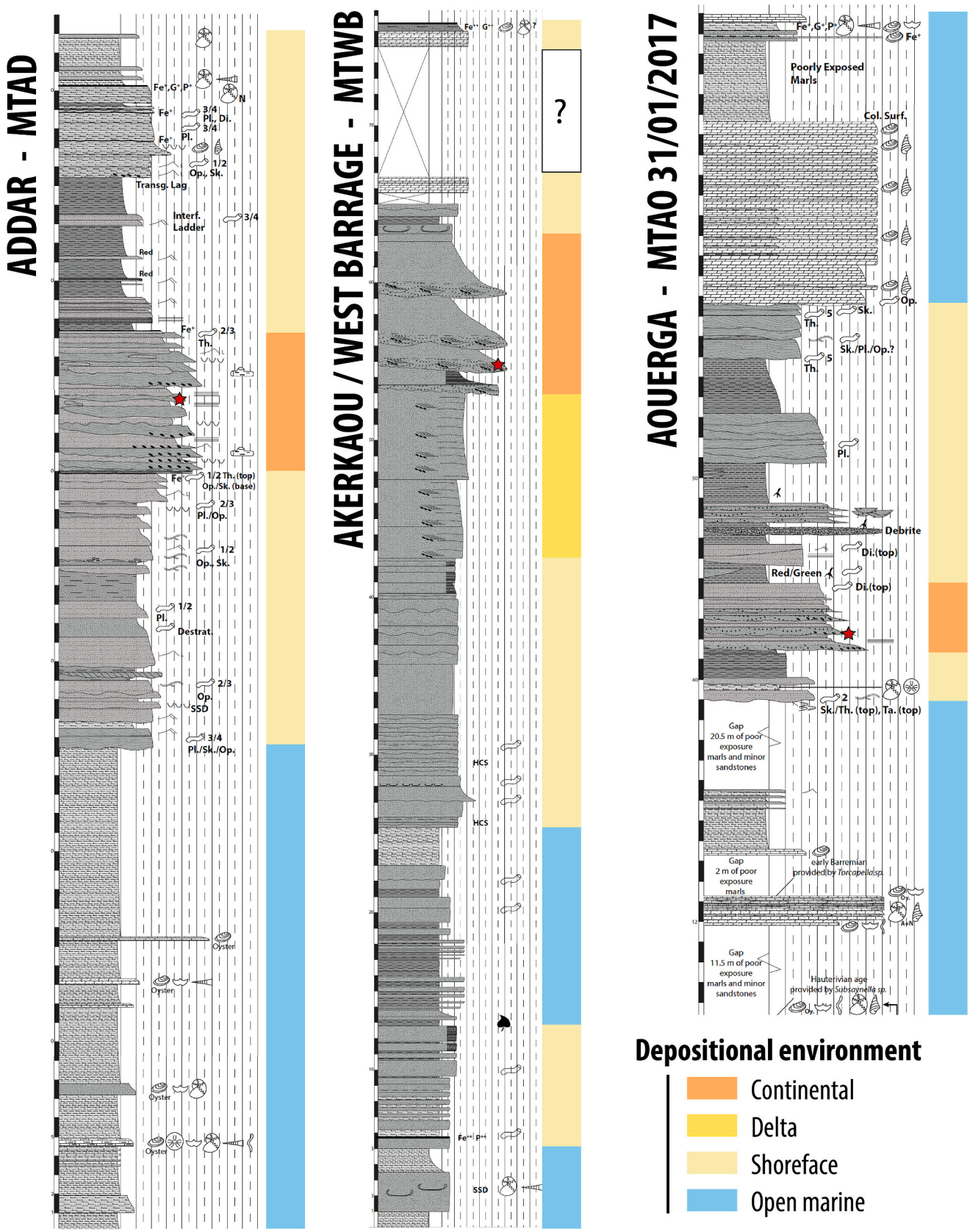

Fig. 16. Stratigraphic logs of the outcrops of Addar, Akerkaou and Aouerga with associated depositional environments from Luber (2017). For details of lithology, sedimentary structures, fossil content, biostratigraphy and depositional environments, see Luber (2017) and references therein.

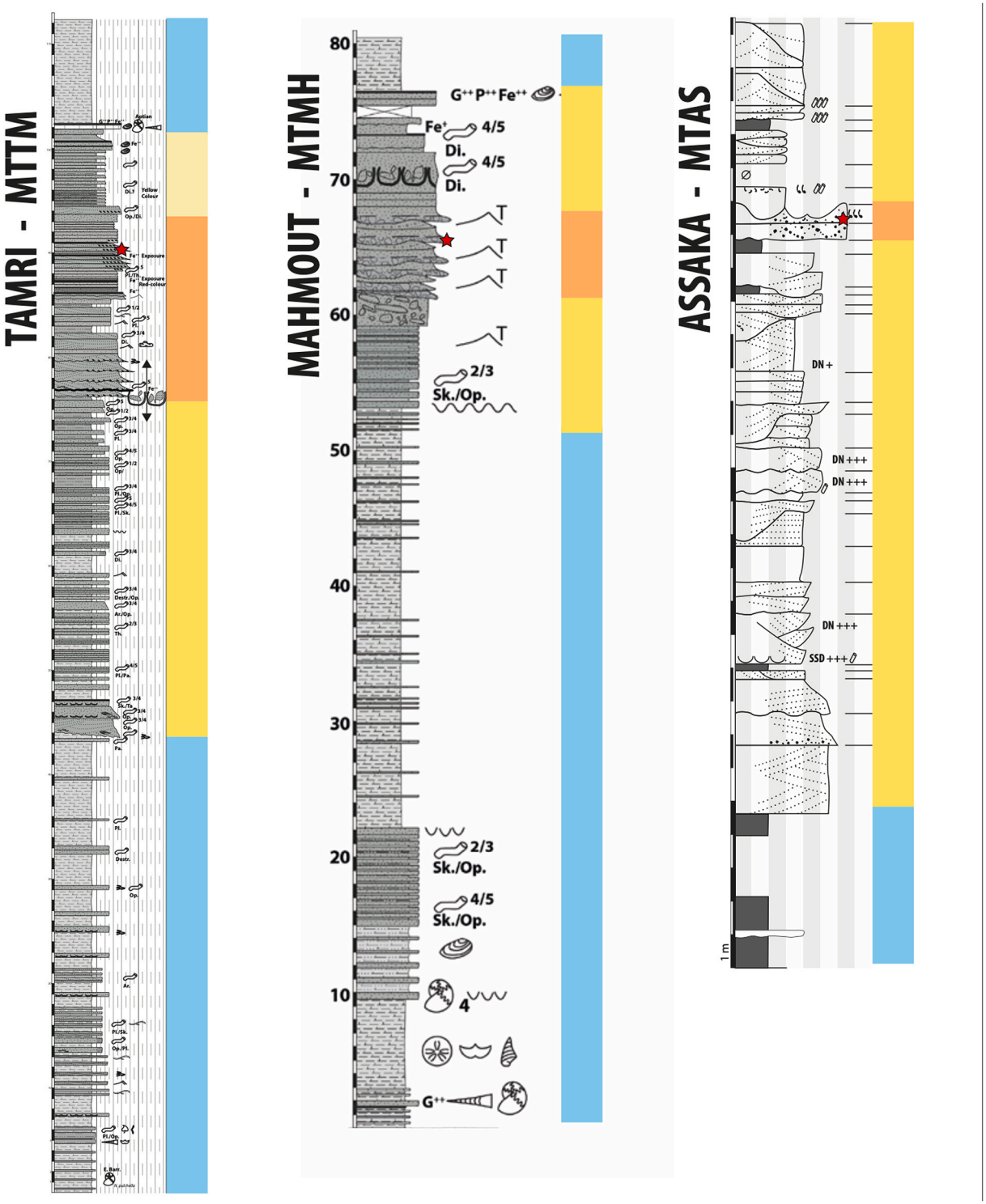

Fig. 17. Stratigraphic logs of the outcrops of Tamri, Mahmout and Assaka with associated depositional environments from Luber (2017). Caption for depositional environments is same as on Fig. 16. For details of lithology, sedimentary structures, fossil content, biostratigraphy and depositional environments, see Luber (2017) and references therein.

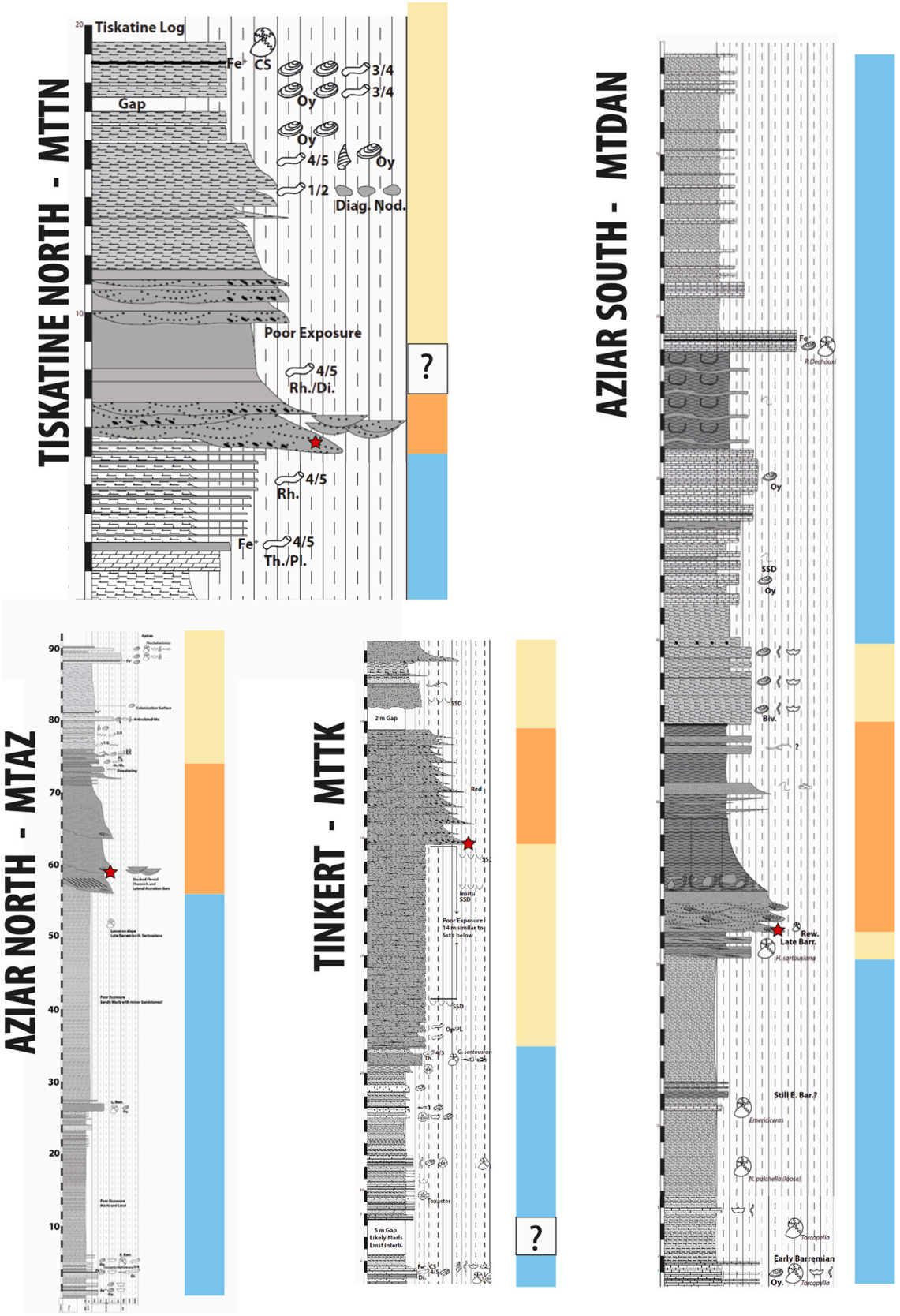

Fig. 18. Stratigraphic logs of the outcrops of Aziar North, Tinkert, Aziar South and Tiskatine North with associated depositional environments from Luber (2017). Caption for depositional environments is same as on Fig. 16. For details of lithology, sedimentary structures, fossil content, biostratigraphy and depositional environments, see Luber (2017) and references therein.

Table 2
Reference of LTT datasets used to constrain burial and exhumation patterns on Fig. 7.

Region [−]	Reference [−]
Western Anti-Atlas	(Charton et al., 2018; Gouiza et al., 2017; Leprêtre, 2015; Ruiz et al., 2011; Sebti, 2011; Sehrt, 2014)
Central Anti-Atlas	(Balestrieri et al., 2009; Ghorbal, 2009; Gouiza et al., 2017; Oukassou et al., 2013)
Eastern Anti-Atlas	(Barbero et al., 2007; Gouiza et al., 2017; Malusà et al., 2007)
MAM/High Atlas	(Balestrieri et al., 2009; Barbero et al., 2007; Domenech, 2015; Ghorbal, 2009)
Western Meseta	(Ghorbal, 2009; Ghorbal et al., 2008; Sabil, 1995; Saddiqi et al., 2009; Sebti et al., 2009)

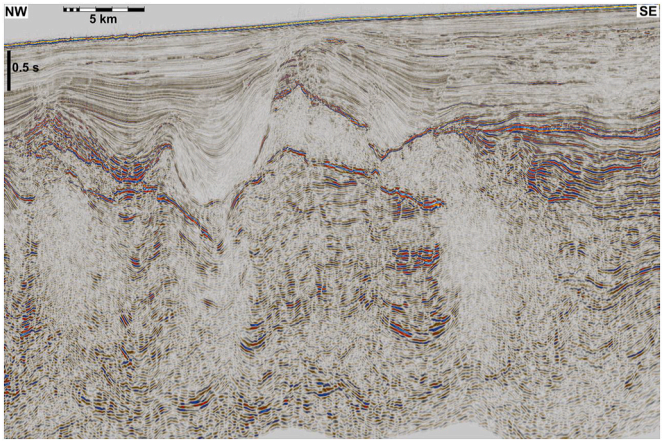

Fig. 19. Uninterpreted seismic line offshore Assaka presented in Fig. 12. The fact that we have those bright (high-amplitude) bodies in between low-amplitude reflectors indicates a different, more sandMalusà et al., 2007-prone interval (given that we are in a clastic-dominated interval). These seismic facies coupled with the channel-like (concave base and generally with a convex top) morphology with internal onlaps and the location within the mini basin axial trough provides a strong argument for the interpretation of deep-water channel-lobe facies (or at least sand-prone intervals).

Table 3
Outcrop coordinates and code name

Outcrop name [−]	Outcrop code [−]	Latitude [dec. Deg.]	Longitude [dec. Deg.]
Tiskatine North	MTTN	30.84342	−9.67121
Assaka	MTAS	30.81406	−9.77168
Aziar North	MTAZ	30.80863	−9.61164
Aziar	MTDAN	30.76080	−9.58976
West Barrage/Akerkaou	MTWB	30.75538	−9.75881
Barrage	MTBR	30.75895	−9.68653
Tinkert	MTTK	30.73577	−9.63322
Mahmout	MTMH	30.72021	−9.80223
Tamri	MTTM	30.70460	−9.82758
Addar	MTAD	30.60226	−9.71919
Aouerga	MTAO	30.59358	−9.64122
Tamzergout	MTTZ	30.55127	−9.55678

Appendix A. Supplementary data

Supplementary data to this article can be found online at https://doi.org/10.1016/j.jafrearsci.2024.105205.

References

Abati, J., Aghzer, A.M., Gerdes, A., Ennih, N., 2010. Detrital zircon ages of Neoproterozoic sequences of the Moroccan Anti-Atlas belt. Precambrian Res. 181, 115–128. https://doi.org/10.1016/j.precamres.2010.05.018.

Accotto, C., Martínez Poyatos, D.J., Azor, A., Talavera, C., Evans, N.J., Jabaloy-Sánchez, A., Azdimousa, A., Tahiri, A., El Hadi, H., 2019. Mixed and recycled detrital zircons in the Paleozoic rocks of the Eastern Moroccan Meseta: paleogeographic inferences. Lithos 73–86. https://doi.org/10.1016/j.lithos.2019.04.011, 338–339.

Adams, A.E., 1979. Sedimentary environments and palaeogeography of the western high atlas, Morocco, during the Middle and late jurassic. Palaeogeogr. Palaeoclimatol. Palaeoecol. 28, 185–196. https://doi.org/10.1016/0031-0182(79)90118-4.

Andersen, T., 2005. Detrital zircons as tracers of sedimentary provenance: limiting conditions from statistics and numerical simulation. Chem. Geol. 216, 249–270. https://doi.org/10.1016/j.chemgeo.2004.11.013.

Andersen, T., Kristoffersen, M., Elburg, M.A., 2016. How far can we trust provenance and crustal evolution information from detrital zircons? A South African case study. Gondwana Res. 34, 129–148. https://doi.org/10.1016/j.gr.2016.03.003.

Aomine, S., Wada, K., 1962. Differential weathering of volcanic ash and pumice, resulting in formation of hydrated halloysite. Am. Mineral. 47, 1024–1048.

Avigad, D., Gerdes, A., Morag, N., Bechstädt, T., 2012. Coupled U-Pb-Hf of detrital zircons of cambrian sandstones from Morocco and sardinia: implications for provenance and precambrian crustal evolution of North Africa. Gondwana Res. 21, 690–703. https://doi.org/10.1016/j.gr.2011.06.005.

Azdimousa, A., Jabaloy-Sánchez, A., Talavera, C., Asebriy, L., González-Lodeiro, F., Evans, N.J., 2019. Detrital zircon U-Pb ages in the Rif Belt (northern Morocco): paleogeographic implications. Gondwana Res. 70, 133–150. https://doi.org/10.1016/j.gr.2018.12.008.

Bailey, E.H., Stevens, R.E., 1960. Selective staining of K-feldspar and plagioclase on rock slabs and thin sections. Am. Mineral. 45, 1020–1025.

Balestrieri, M.L., Moratti, G., Bigazzi, G., Algouti, A., 2009. Neogene exhumation of the Marrakech High Atlas (Morocco) recorded by apatite fission-track analysis. Terra. Nova 21, 75–82. https://doi.org/10.1111/j.1365-3121.2008.00857.x.

Barbero, L., Teixell, A., Arboleya, M.L., del Rio, P., Reiners, P.W., Bougadir, B., 2007. Jurassic-to-present thermal history of the central High Atlas (Morocco) assessed by low-temperature thermochronology. Terra. Nova 19, 58–64. https://doi.org/10.1111/j.1365-3121.2006.00715.x.

Barbero, L., Jabaloy, A., Gómez-Ortiz, D., Pérez-Peña, J.V., Rodríguez-Peces, M.J., Tejero, R., Estupiñán, J., Azdimousa, A., Vázquez, M., Asebriy, L., 2011. Evidence for surface uplift of the Atlas Mountains and the surrounding peripheral plateaux: combining apatite fission-track results and geomorphic indicators in the Western Moroccan Meseta (coastal Variscan Paleozoic basement). Tectonophysics 502, 90–104. https://doi.org/10.1016/j.tecto.2010.01.005.

Beauchamp, J., 1988. Triassic sedimentation and rifting in the high atlas. Dev. Geotectonics 22, 477–497.

Behrens, M., Krumsiek, K., Meyer, D.E., Schäfer, E.A., Siehl, A., Stets, J., Thein, J., Wurster, P., 1978. Sedimentationsabläufe im Atlas-Golf (Kreide Küstenbecken Marokko). Geol. Rundsch. 67, 424–453. https://doi.org/10.1007/BF01802799.

Bensalah, M.K., Youbi, N., Mata, J., Madeira, J., Martins, L., El Hachimi, H., Bertrand, H., Marzoli, A., Bellieni, G., Doblas, M., Font, E., 2013. The Jurassic–Cretaceous basaltic magmatism of the Oued El-Abid syncline (High Atlas, Morocco): Physical volcanology, geochemistry and geodynamic implications. Journal of African Earth Sciences 81, 60–81. https://doi.org/10.1016/j.jafrearsci.2013.01.004.

Bertotti, G., Gouiza, M., 2012. Post-rift vertical movements and horizontal deformations in the eastern margin of the Central Atlantic: Middle Jurassic to Early Cretaceous evolution of Morocco. Int. J. Earth Sci. 101, 2151–2165. https://doi.org/10.1007/s00531-012-0773-4.

Boher, M., Abouchami, W., Michard, A., Albarede, F., Arndt, N.T., 1992. Crustal growth in west Africa at 2.1 Ga. J. Geophys. Res. 97, 345–369. https://doi.org/10.1029/91JB01640.

Butt, A., 1982. Micropalaeontological bathymetry of the Cretaceous of western Morocco. Palaeogeogr. Palaeoclimatol. Palaeoecol. 37, 235–275.

Charton, R., 2018. Phanerozoic Vertical Movements in Morocco Phanerozoic Vertical Movements in Morocco. PhD Thesis. TU Delft. https://osf.io/preprints/thesiscommons/av2ne.

Charton, R., Bertotti, G., Arantegui, A., Bulot, L., 2018. The Sidi Ifni transect across the rifted margin of Morocco (Central Atlantic): vertical movements constrained by low-temperature thermochronology. J. Afr. Earth Sci. 141, 22–32. https://doi.org/10.1016/j.jafrearsci.2018.01.006.

Charton, R., Bertotti, G., Duval-Arnould, A., Storms, J.E.A., Redfern, J., 2021a. Low-temperature thermochronology as a control on vertical movements for semi-quantitative Source-to-Sink analysis: a case study for the Permian to Neogene of Morocco and surroundings. Basin Res. 33, 1337–1383. https://doi.org/10.1111/bre.12517.

Charton, R., Kluge, C., Fernandez-Blanco, D., Duval-Arnould, A., Bryers, O., Redfern, J., Bertotti, J., 2021b. Syn-depositional Mesozoic siliciclastic pathways on the Moroccan Atlantic margin linked to evaporite mobilisation. Mar. Petrol. Geol. 128, 105018 https://doi.org/10.1016/j.marpetgeo.2021.105018.

Domenech, M., 2015. Rift Opening and Inversion in the Marrakech High Atlas : Integrated Structural and Thermochronologic Study. PhD Thesis. Universitat Autònoma de Barcelona.

Domènech, M., Teixell, A., Stockli, D.F., 2016. Magnitude of rift-related burial and orogenic contraction in the Marrakech High Atlas revealed by zircon (U-Th)/He thermochronology and thermal modelling. Tectonics 35, 2609–2635. https://doi.org/10.1002/2016TC004283.

Domènech, M., Stockli, D.F., Teixell, A., 2018. Detrital zircon U–Pb provenance and palaeogeography of Triassic rift basins in the Marrakech High Atlas. Terra. Nova 30, 310–318. https://doi.org/10.1111/ter.12340.

El Houicha, M., Pereira, M.F., Jouhari, A., Gama, C., Ennih, N., Fekkak, A., Ezzouhairi, H., El Attari, A., Silva, J.B., 2018. Recycling of the Proterozoic crystalline basement in the Coastal Block (Moroccan Meseta): new insights for understanding the geodynamic evolution of the northern peri-Gondwanan realm. Precambrian Res. 306, 129–154. https://doi.org/10.1016/j.precamres.2017.12.039.

Espejo, I.S., Lopez-Gamundi, O.R., 1994. Source versus depositional controls on sandstone composition in a foreland basin: the el imperial formation (mid carboniferous-lower permian), san rafael basin, western Argentina. J. Sediment. Res. A64, 8–16.

Fabuel-Perez, I., Hodgetts, D., Redfern, J., 2009. A new approach for outcrop characterization and geostatistical analysis of a low-sinuosity fluvial-dominated succession using digital outcrop models: upper Triassic Oukaimeden Sandstone Formation, central High Atlas, Morocco. Am. Assoc. Petrol. Geol. Bull. 93, 795–827. https://doi.org/10.1306/02230908102.

Ferry, Serge, Masrour, Moussa, Grosheny, Danièle, 2007. Excursion Le Crétacé de la marge atlantique marocaine (région ''Agadir) (1-7 septembre 2007). Excursion du Groupe Français du Crétacé. Série« "Excursion »", 75 pp. ⟨hal-00686791⟩.

Frau, C., Tendil, A.J.-B., Pohl, A., Lanteaume, C., 2020. Revising the timing and causes of the Urgonian rudistid-platform demise in the Mediterranean Tethys. Global Planet. Change 187, 103–124.

Frizon de Lamotte, D., Zizi, M., Missenard, Y., Hafid, M., El Azzouzi, M., Maury, R., Charriere, A., Taki, Z., Benammi, M., Michard, A., 2008. The atlas system. Continental Evolution: the Geology of Morocco: Structure, Stratigraphy, and Tectonics of the Africa-Atlantic-Mediterranean Triple Junction. Springer, Berlin, pp. 133–202.

Gallagher, K., Brown, R., Johnson, C., 1998. Fission track analysis and its applications to geological problems. Annu. Rev. Earth Planet Sci. 26, 519–572. https://doi.org/10.1146/annurev.earth.26.1.519.

Gärtner, A., Youbi, N., Villeneuve, M., Sagawe, A., Hofmann, M., Mahmoudi, A., Boumehdi, M.A., Linnemann, U., 2017. The zircon evidence of temporally changing sediment transport—the NW Gondwana margin during Cambrian to Devonian time (Aoucert and Smara areas, Moroccan Sahara). Int. J. Earth Sci. 1–23. https://doi.org/10.1007/s00531-017-1457-x.

Gärtner, A., Youbi, N., Villeneuve, M., Linnemann, U., Sagawe, A., Hofmann, M., Zieger, J., Mahmoudi, A., Boumehdi, M.A., 2018. Provenance of detrital zircon from siliciclastic rocks of the sebkha gezmayet unit of the adrar souttouf massif (Moroccan Sahara) – palaeogeographic implications. Compt. Rendus Geosci. 350, 255–266. https://doi.org/10.1016/j.crte.2018.06.004.

Garzanti, E., 2019. Petrographic classification of sand and sandstone. Earth Sci. Rev. 192, 545–563. https://doi.org/10.1016/j.earscirev.2018.12.014.

Garzanti, E., Andò, S., 2007. Chapter 20 heavy mineral concentration in modern sands: implications for provenance interpretation. Dev. Sedimentol. 58, 517–545. https://doi.org/10.1016/S0070-4571(07)58020-9.

Gasquet, D., Ennih, N., Liégeois, J.-P., Soulaimani, A., Michard, A., 2008a. The pan-African belt. Lect. Notes Earth Sci 116, 33–64. https://doi.org/10.1007/978-3-540-77076-3_2.

Ghienne, J.F., Benvenuti, A., El Houicha, M., Girard, F., Kali, E., Khoukhi, Y., Langbour, C., Magna, T., Míková, J., Moscariello, A., Schulmann, K., 2018. The impact of the end-Ordovician glaciation on sediment routing systems: a case study from the Meseta (northern Morocco). Gondwana Res. 63, 169–178. https://doi.org/10.1016/j.gr.2018.07.001.

Ghorbal, B., 2009. Mesozoic to Quaternary Thermotectonic Evolution of Morocco (NW Africa). Vrije Universiteit Amsterdam.

Ghorbal, B., Bertotti, G., Foeken, J., Andriessen, P., 2008. Unexpected Jurassic to Neogene vertical movements in 'stable' parts of NW Africa revealed by low temperature geochronology. Terra. Nova 20, 355–363. https://doi.org/10.1111/j.1365-3121.2008.00828.x.

Giraud, F., Kassab, W.H., Robert, E., Jaillard, E., Spangenberg, J.E., Masrour, M., Hammed, M.S., Aly, M.F., El Hariri, K., 2020. Integrated stratigraphy of the latest Barremian–early Albian interval in the western part of the Tethyan margin: new data from the Essaouira-Agadir Basin (Western Morocco). Newsl. Stratigr. 54 (1), 43–78. https://doi.org/10.1127/nos/2020/0603.

Gouiza, M., Charton, R., Bertotti, G., Andriessen, P., Storms, J.E.A., 2017. Post-Variscan evolution of the Anti-Atlas belt of Morocco constrained from low-temperature geochronology. Int. J. Earth Sci. 106, 593–616. https://doi.org/10.1007/s00531-016-1325-0.

Guedes, C.C.F., Giannini, P.C.F., Nascimento, D.R., Sawakuchi, A.O., Tanaka, A.P.B., Rossi, M.G., 2011. Controls of heavy minerals and grain size in a Holocene regressive barrier (Ilha Comprida, southeastern Brazil). J. South Am. Earth Sci. 31, 110–123. https://doi.org/10.1016/j.jsames.2010.07.007.

Hafid, M., Zizi, M., Bally, A.W., Ait Salem, A., 2006. Structural styles of the western onshore and offshore termination of the High Atlas, Morocco. Compt. Rendus Geosci. 338, 50–64. https://doi.org/10.1016/j.crte.2005.10.007.

Haq, B.U., 2013. Cretaceous eustasy revisited. Global Planet. Change 113, 44–58. https://doi.org/10.1016/j.gloplacha.2013.12.007.

Helland-Hansen, W., Sømme, T.O., Martinsen, O.J., Lunt, I., Thurmond, J., 2016. Deciphering earth's natural hourglasses: perspectives on source-to-sink analysis. J. Sediment. Res. 86, 1008–1033. https://doi.org/10.2110/jsr.2016.56.

Hoepffner, C., Soulaimani, A., Piqué, A., 2005. The Moroccan hercynides. J. Afr. Earth Sci. 43, 144–165. https://doi.org/10.1016/j.jafrearsci.2005.09.002.

Hoepffner, C., Houari, M.R., Bouabdelli, M., 2006. Tectonics of the North african variscides (Morocco, western Algeria): an outline. Compt. Rendus Geosci. 338, 25–40. https://doi.org/10.1016/J.CRTE.2005.11.003.

Hubert, J.F., 1962. A zircon-tourmaline-rutile maturity index and the interdependence of the composition of heavy mineral assemblages with the gross composition and texture of sandstones. J. Sediment. Res. 32, 440–450. https://doi.org/10.1306/74d70ce5-2b21-11d7-8648000102c1865d.

Ingersoll, R.V., Bullard, T.F., Ford, R.L., Grimm, J.P., Pickle, J.D., Sares, S.W., 1984. The effect of grain size on detrital modes: a test of the Gazzi-Dickinson point-counting method. J. Sediment. Petrol. 54, 103–116.

Jaillard, E., Kassab, W.H., Giraud, F., Robert, E., Masrour, M., Bouchaou, L., El Hariri, K., Hammed, M.S., Aly, M.F., 2019. Aptian–early Albian sedimentation in the Essaouira-Agadir basin, western Morocco. Cretac. Res. 102, 59–80. https://doi.org/10.1016/j.cretres.2019.04.008.

Jaillard, E., Al Yacoubi, L., Reboulet, S., Robert, E., Masrour, M., Bouchaou, L., Giraud, F., El Hariri, K., 2019a. Late barremian eustacy and tectonism in the western high atlas (Essaouira-Agadir Basin), Morocco. Cretac. Res. 93, 225–244. https://doi.org/10.1016/j.cretres.2018.08.002.

Kenny, G.G., Sullivan, G.J.O., Alexander, S., Simms, M.J., Chew, D.M., Kamber, B.S., 2019. On the track of a Scottish impact structure: a detrital zircon and apatite provenance study of the Stac Fada Member and wider Stoer Group, NW Scotland. Geol. Mag. 156, 1863–1876.

Lanari, R., Faccenna, C., Fellin, M.G., Essaifi, A., Nahid, A., Medina, F., Youbi, N., 2020. Tectonic evolution of the western high atlas of Morocco: oblique convergence, reactivation, and transpression. Tectonics 39, 1–27. https://doi.org/10.1029/2019TC005563.

Le Roy, P., Piqué, A., 2001. Triassic-Liassic western Moroccan synrift basins in relation to the Central Atlantic opening. Mar. Geol. 172, 359–381. https://doi.org/10.1016/S0025-3227(00)00130-4.

Leprêtre, R., 2015. Evolution phanérozoïque du Craton Ouest Africain et de ses bordures Nord et Ouest. Université Paris Sud - Paris XI.

Leprêtre, R., Missenard, Y., Barbarand, J., Gautheron, C., Jouvie, I., Saddiqi, O., 2018. Polyphased inversions of an intracontinental rift: case study of the Marrakech high atlas, Morocco. Tectonics 37, 818–841. https://doi.org/10.1002/2017TC004693.

Lovell-Kennedy, J., Roquette, E., Schröder, S., Redfern, J., 2023. 'I hate sand… it gets everywhere'—phanerozoic sedimentary recycling from NW Africa. Basin Res. 35 (1), 187–213. https://doi.org/10.1111/bre.12709.

Luber, T.L., 2017. Integrated Analysis of Lower Cretaceous Stratigraphy and Depositional Systems : the Essaouira-Agadir Basin of Morocco. PhD Thesis. University of Manchester. https://www.librarysearch.manchester.ac.uk/permalink/44MAN_INST/bofker/alma9929778717587016 31.

Luber, T.L., Bulot, L.G., Redfern, J., Frau, C., Arantegui, A., Masrour, M., 2017. A revised ammonoid biostratigraphy for the aptian of NW Africa: Essaouira-Agadir Basin, Morocco. Cretac. Res. 79, 12–34. https://doi.org/10.1016/j.cretres.2017.06.020.

Luber, T.L., Bulot, L.G., Redfern, J., Nahim, M., Jeremiah, J., Simmons, M., Bodin, S., Frau, C., Bidgood, M., Masrour, M., 2019. A revised chronostratigraphic framework for the Aptian of the Essaouira-Agadir Basin, a candidate type section for the NW African Atlantic Margin. Cretac. Res. 93, 292–317. https://doi.org/10.1016/j.cretres.2018.09.007.

Mader, N.K., Redfern, J., El Ouataoui, M., 2017. Sedimentology of the Essaouira Basin (Meskala Field) in context of regional sediment distribution patterns during upper Triassic pluvial events. J. Afr. Earth Sci. 130, 293–318. https://doi.org/10.1016/j.jafrearsci.2017.02.012.

Malusà, M.G., Polino, R., Feroni, A.C., Ellero, A., Ottria, G., Baidder, L., Musumeci, G., 2007. Post-Variscan tectonics in eastern anti-atlas (Morocco). Terra. Nova 19, 481–489. https://doi.org/10.1111/j.1365-3121.2007.00775.x.

Marzoli, A., Davies, J.H.F.L., Youbi, N., Merle, R., Corso, J.D., Dunkley, D.J., Fioretti, A. M., Bellieni, G., Medina, F., Wotzlaw, J.-F., McHone, G., Font, E., Bensalah, M.K., 2017. Proterozoic to mesozoic evolution of north-west Africa and peri-gondwana microplates: detrital zircon ages from Morocco and Canada. Lithos 278–281, 229–239. https://doi.org/10.1016/j.lithos.2017.01.016.

Marzoli, A., Bertrand, H., Youbi, N., Callegaro, S., Merle, R., Reisberg, L., Chiaradia, M., Brownlee, S.I., Jourdan, F., Zanetti, A., Davies, J.H.F.L., Cuppone, T., Mahmoudi, A., Medina, F., Renne, P.R., Bellieni, G., Crivellari, S., El Hachimi, H., Bensalah, M.K., Meyzen, C.M., Tegner, C., 2019. The central atlantic magmatic province (CAMP) in Morocco. J. Petrol. 60, 945–996. https://doi.org/10.1093/petrology/egz021.

Medina, F., 1991. Superimposed extensional tectonics in the Argana Triassic formations (Morocco), related to the early rifting of the Central Atlantic. Geol. Mag. 128, 525–536. https://doi.org/10.1017/S0016756800018665.

Medina, F., 1995. Syn- and postrift evolution of the El Jadida – Agadir basin (Morocco): constraints for the rifting models of the central Atlantic. Can. J. Earth Sci. 32, 1273–1291. https://doi.org/10.1139/e95-104.

Michard, A., Frizon de Lamotte, D., Saddiqi, O., Chalouan, A., 2008a. An outline of the geology of Morocco. Lect. Notes Earth Sci. 116, 1–31. https://doi.org/10.1007/978-3-540-77076-3_1.

Michard, A., Hoepffner, C., Soulaimani, A., Baidder, L., 2008b. The variscan belt. Cont. Evol. Geol. Morocco 65–132. https://doi.org/10.1007/978-3-540-77076-3_3.

Michard, A., de Lamotte, D.F., Hafid, M., Charrière, A., Haddoumi, H., Ibouh, H., 2013. Comment on "The Jurassic–Cretaceous basaltic magmatism of the Oued El-Abid syncline (High Atlas, Morocco): Physical volcanology, geochemistry and geodynamic implications"' by Bensalah et al., J. Afr. Earth Sci. 81 (2013) 60–81. J. Afr. Earth Sci. 88, 101–105. https://doi.org/10.1016/j.jafrearsci.2013.08.009.

Missenard, Y., Saddiqi, O., Barbarand, J., Leturmy, P., Ruiz, G., El Haimer, F.Z., de Lamotte, D.F., 2008. Cenozoic denudation in the Marrakech high atlas, Morocco: insight from apatite fission-track thermochronology. Terra. Nova 20, 221–228. https://doi.org/10.1111/j.1365-3121.2008.00810.x.

Morton, A.C., 1984. Stability of detrital heavy minerals in tertiary sandstones from the North sea basin. Clay Miner. 19, 287–308. https://doi.org/10.1180/claymin.1984.019.3.04.

Morton, A.C., 2012. Value of heavy minerals in sediments and sedimentary rocks for provenance, transport history and stratigraphic correlation. In: Quantitative Mineralogy and Microanalysis of Sediments and Sedimentary Rocks: Mineralogical Association of Canada Short Course, pp. 133–165.

Morton, A.C., Hallsworth, C., 2007. Chapter 7 stability of detrital heavy minerals during burial diagenesis. Dev. Sedimentol. 58, 215–245. https://doi.org/10.1016/S0070-4571(07)58007-6.

Mrini, Z., Rafi, A., Duthou, J.-L., Vidal, P., 1992. Chronologie Rb-Sr des granitoides hercyniens du Maroc : conséquences. Bull. la Soc. Geol. Fr. 163, 281–291.

Nouidar, M., 2001. Facies and sequence stratigraphy of an estuarine incised-valley fill: lower aptian Bouzergoun Formation, Agadir Basin, Morocco. Cretac. Res. 22 (1), 93–104.

Nouidar, M., 2002. Facies and sequence stratigraphy of a Late Barremian wave-dominated deltaic deposit, Agadir Basin, Morocco. Sediment. Geol. 150 (3–4), 375–384.

Nouidar, M., Chellai, E.H., 2000. Facies and sequence stratigraphy of upper barremian-lower aptian Bouzergoun Formation, Agadir Basin, Morocco. Afr. Geosci. Rev. 7, 327–340. https://doi.org/10.1006/cres.2000.0239.

Oukassou, M., Saddiqi, O., Barbarand, J., Sebti, S., Baidder, L., Michard, A., 2013. Post-Variscan exhumation of the Central Anti-Atlas (Morocco) constrained by zircon and apatite fission-track thermochronology. Terra. Nova 25, 151–159. https://doi.org/10.1111/ter.12019.

O'Sullivan, G., Chew, D., Kenny, G., Henrichs, I., Mulligan, D., 2020. The trace element composition of apatite and its application to detrital provenance studies. Earth Sci. Rev. 201, 103044 https://doi.org/10.1016/j.earscirev.2019.103044.

Paton, C., Woodhead, J.D., Hellstrom, J.C., Hergt, J.M., Greig, A., Maas, R., 2010. Improved laser ablation U-Pb zircon geochronology through robust downhole fractionation correction. G-cubed 11. https://doi.org/10.1029/2009GC002618.

Paton, C., Hellstrom, J., Paul, B., Woodhead, J., Hergt, J., 2011. Iolite: freeware for the visualisation and processing of mass spectrometric data. J. Anal. At. Spectrom. 26, 2508–2518. https://doi.org/10.1039/c1ja10172b.

Perez, N.D., Teixell, A., Gómez-Gras, D., Stockli, D.F., 2019. Reconstructing extensional basin architecture and provenance in the Marrakech high atlas of Morocco: implications for rift basins and inversion tectonics. Tectonics 38, 1584–1608. https://doi.org/10.1029/2018TC005413.

Pichel, L.M., 2018. Tectono-Stratigraphic Evolution Associated with Salt Tectonics along Atlantic Margins: Effects of Pre-salt Relief and Regional Events. The University of Manchester (United Kingdom). https://pure.manchester.ac.uk/ws/portalfiles/portal/157709781/FULL_TEXT.PDF.

Pichel, L.M., Huuse, M., Redfern, J., Finch, E., 2019. The influence of base-salt relief, rift topography and regional events on salt tectonics offshore Morocco. Mar. Petrol. Geol. 103, 87–113. https://doi.org/10.1016/j.marpetgeo.2019.02.007.

Potrel, A., Peucat, J.-J., Fanning, M., Auvray, B., Burg, J., Caruba, C., 2007. 3.5 Ga old terranes in the West african craton, Mauritania. J. Geol. Soc. London. https://doi.org/10.1144/gsjgs.153.4.0507.

Reboulet, S., Jaillard, E., Shmeit, M., Giraud, F., Masrour, M., Spangenberg, J.E., 2022. Biostratigraphy, carbon isotope and sequence stratigraphy of south tethyan valanginian successions in the Essaouira-Agadir Basin (Morocco). Cretac. Res. 140, 105341 https://doi.org/10.1016/j.cretres.2022.105341.

Rey, J., Canerot, J., Peybernes, B., Taj-Eddine, K., Rahhali, K., Thieuloy, J.P., 1986a. Le Crétacé inférieur de la région d'Essaouira : données biostratigraphiques et évolutions. Rev. la Fac. des Sci. Marrakech no spécial 413–441.

Rey, J., Canerot, J., Rocher, A., Taj-Eddine, K., Thieuloy, J.P., 1986b. Le Crétacé inférieur sur le versant nord du Haut-Atlas (région d'Imi n'Tanout et Amizmiz) données biostratigraphiques et évolutions sédimentaires. Rev. la Fac. des Sci. Marrakech 183, 393–441.

Rey, J., Canérot, J., Peybernès, B., Taj-Eddine, K., Thieuloy, J.P., 1988. Lithostratigraphy, biostratigraphy and sedimentary dynamics of the Lower Cretaceous deposits on the northern side of the western High Atlas (Morocco). Cretac. Res. 9, 141–158. https://doi.org/10.1016/0195-6671(88)90014-6.

Ruiz, G.M.H., Sebti, S., Negro, F., Saddiqi, O., Frizon de Lamotte, D., Stockli, D., Foeken, J., Stuart, F., Barbarand, J., Schaer, J.P., 2011. From central Atlantic continental rift to Neogene uplift - western Anti-Atlas (Morocco). Terra. Nova 23, 35–41. https://doi.org/10.1111/j.1365-3121.2010.00980.x.

Saadi, M., Hilali, E.A., Bensaid, M., Boudda, A., Dahmani, M., 1985. Carte Géologique de Maroc. Ministère l'Énergie des Mines, Dir. la Géologie.

Sabil, N., 1995. La datation par traces de fission: aspects méthodologiques et applications thermochronologiques en contexte alpin et de marge continentale. PhD Thesis. Université Joseph Fourier - Grenoble I.

Saddiqi, O., El Haimer, F.Z., Michard, A., Barbarand, J., Ruiz, G.M.H., Mansour, E.M., Leturmy, P., Frizon de Lamotte, D., 2009. Apatite fission-track analyses on basement granites from south-western Meseta, Morocco: paleogeographic implications and interpretation of AFT age discrepancies. Tectonophysics 475, 29–37. https://doi.org/10.1016/j.tecto.2009.01.007.

Sahabi, M., Aslanian, D., Olivet, J.-L., 2004. Un nouveau point de départ pour l'histoire de l'Atlantique central. Compt. Rendus Geosci. 336, 1041–1052.

Schlische, R.W., Withjack, M.O., Olsen, P.E., 2013. Relative timing of CAMP, rifting, continental breakup, and basin inversion: tectonic significance. Geophys. Monogr. 136, 33–59. https://doi.org/10.1029/136GM03.

Scotese, C.R., 2016. PALEOMAP PaleoAtlas for GPlates and the PaleoData Plotter Program [WWW Document]. PALEOMAP Proj.

Sebti, S., 2011. Mouvements verticaux de l'Anti-Atlas Occidental marocain (Kerdous and Ifni): Thermochronologie par traces de fission. PhD Thesis. Université Hassan II.

Sebti, S., Saddiqi, O., El Haimer, F.Z., Michard, A., Ruiz, G., Bousquet, R., Baidder, L., Frizon de Lamotte, D., 2009. Vertical movements at the fringe of the West African Craton: first zircon fission track datings from the Anti-Atlas Precambrian basement, Morocco. Compt. Rendus Geosci. 341, 71–77. https://doi.org/10.1016/j.crte.2008.11.006.

Sehrt, M., 2014. Variscan to Neogene long-term landscape evolution at the Moroccan passive continental margin (Tarfaya Basin and western anti-Atlas). PhD Thesis. Ruprecht-Karls-Universität Heidelberg.

Sláma, J., Košler, J., Condon, D.J., Crowley, J.L., Gerdes, A., Hanchar, J.M., Horstwood, M.S.A., Morris, G.A., Nasdala, L., Norberg, N., Schaltegger, U., Schoene, B., Tubrett, M.N., Whitehouse, M.J., 2008. Plešovice zircon - a new natural reference material for U-Pb and Hf isotopic microanalysis. Chem. Geol. 249, 1–35. https://doi.org/10.1016/j.chemgeo.2007.11.005.

Sømme, T.O., Helland-Hansen, W., Martinsen, O.J., Thurmond, J.B., 2009. Relationships between morphological and sedimentological parameters in source-to-sink systems: a basis for predicting semi-quantitative characteristics in subsurface systems. Basin Res. 21, 361–387. https://doi.org/10.1111/j.1365-2117.2009.00397.x.

Soulaimani, A., Ouanaimi, H., Saddiqi, O., Baidder, L., Michard, A., 2018. The anti-atlas pan-african belt (Morocco): overview and pending questions. Compt. Rendus Geosci. 350, 279–288. https://doi.org/10.1016/j.crte.2018.07.002.

Spear, F.S., Pyle, J.M., 2002. Apatite, monazite, and xenotime in metamorphic rocks. Rev. Mineral. Geochem. 48, 293–335.

Stephan, T., Kroner, U., Romer, R.L., 2019. The pre-orogenic detrital zircon record of the Peri-Gondwanan crust. Geol. Mag. 156, 281–307. https://doi.org/10.1017/S0016756818000031.

Sudo, T., 1954. Clay mineralogical aspects of alteration of volcanic glass in Japan. Clay Miner. Bull. 2, 96–105.

Tari, G., Jabour, H., Tari, G., Jabour, H., 2014. Salt tectonics along the Atlantic margin of Morocco Salt tectonics along the Atlantic margin of Morocco. Conjug. Divergent Margins 337–353. https://doi.org/10.1144/SP369.23.

Ulmer-Scholle, D.S., Scholle, P.A., Schieber, J., Raine, R.J., 2015. A Color Guide to the Petrography of Sandstones, Siltstones, Shales and Associated Rocks. American Association of Petroleum Geologists.

Vermeesch, P., 2018. IsoplotR: a free and open toolbox for geochronology. Geosci. Front. 9, 1479–1493. https://doi.org/10.1016/j.gsf.2018.04.001.

Wiedenbeck, M., Allé, P., Corfu, F., Griffin, W.L., Meier, M., Oberli, F., Quadt, A.V.O.N., Roddick, J.C., Spiegel, W., 1995. Three natural zircon standards for U-Th-Pb, Lu-Hf, trace element and ree analyses. Geostand. Newsl. 19, 1–23. https://doi.org/10.1111/j.1751-908X.1995.tb00147.x.

Wiedmann, J., Butt, A., Einsele, G., 1978. Vergleich von marokkanischen Kreide-Küstenaufschlüssen und Tiefseebohrungen (DSDP): stratigraphie, Paläoenvironment und Subsidenz an einem passiven Kontinentalrand. Geol. Rundsch. 67, 454–508. https://doi.org/10.1007/BF01802800.

Wipf, M., Glasmacher, U.A., Stockli, D.F., Emmerich, A., Bechstädt, T., Baur, H., 2010. Reconstruction of the differentiated long-term exhumation history of Fuerteventura, Canary Islands, Spain, through fission-track and (U-Th-Sm)/He data. Int. J. Earth Sci. 99, 675–686. https://doi.org/10.1007/s00531-008-0415-z.

Zühlke, R., Bouaouda, M.S., Ouajhain, B., Bechstädt, T., Leinfelder, R., 2004. Quantitative Meso-/Cenozoic development of the eastern central Atlantic continental shelf, western High Atlas, Morocco. Mar. Petrol. Geol. 21 (2), 225–276. https://doi.org/10.1016/j.marpetgeo.2003.11.014.